

Study on Additively Manufactured Antennas for Wearables and Bio-medical Applications

by

Sanjee Lamsal

Submitted in Partial Fulfillment of the Requirements

for the Degree of

Master of Science in Engineering

in the

Electrical Engineering
Program

YOUNGSTOWN STATE UNIVERSITY

May 2023

Study on Additively Manufactured Antennas for Wearables and Bio-medical Applications

Sanjee Lamsal

I hereby release this thesis to the public. I understand that this thesis will be made available from the OhioLINK ETD Center and the Maag Library Circulation Desk for public access. I also authorize the University or other individuals to make copies of this thesis as needed for scholarly research.

Signature:

Sanjee Lamsal, Student Date

Approvals:

Dr. Vamsi Borra, Thesis Advisor Date

Dr. Pedro Cortes, Committee Member Date

Dr. Srikanth Itapu, Committee Member Date

Prof. Ghassan Salim, Committee Member Date

Dr. Salvatore A. Sanders, Dean of Graduate Studies Date

ABSTRACT

Design and additive manufacturing of four different antennas that operate at microwave frequency is proposed. The designs were prototyped on flexible FR4 substrates to make them suitable for wearable sensors and biomedical applications. Contact and non-contact printing methods for antenna fabrication using screen printing and aerosol jet printing (AJP), respectively, were extensively studied as part of this research. Ansys High Frequency Structural Simulator (HFSS) was used to design and simulate the antenna characteristics. Nanoparticle silver ink, of ~10nm size, was used to fabricate antennas under AJP method. In addition, a screen-printing approach using copper paste was used to fabricate antennas. A vector network analyzer (VNA) was used to experimentally verify the nature of fabricated samples. The reflection coefficient (S11) and radiation patterns for the simulated design and fabricated samples were found to align closely. A return loss of -10 dB was achieved for the wide range of operating frequency. This demonstrates the effectiveness of the proposed antennas. Compact sizing, simplicity of manufacturing, a larger impedance spectrum, simple design, and high performance are some of the major advantages of the proposed additive manufacturing method.

ACKNOWLEDGEMENTS

I want to express my profound thanks to my adviser, Dr. Vamsi Borra, for his guidance and insightful advice throughout the research. His expertise and understanding were invaluable in accomplishing this thesis. I would like to extend my gratitude to my committee members Dr. Pedro Cortes and Prof. Ghassan Salim for their valuable time and encouragement, and Dr. Srikanth Itapu for his knowledge and feedback which has helped in shaping the research.

I also want to convey my thanks to the Department of Electrical and Computer Engineering faculty members for their continuous support and guidance during my studies at Youngstown State University. My warmest thanks to all my colleagues for the helpful discussion and moral support over the last two years.

For all the financial support to complete this thesis, I would like to thank U.S. Air Force Research Laboratories Assured Digital Microelectronics Education and Training Ecosystem (ADMETE) project.

I express my final thanks to my family: my grandparents, whose personal life experiences and stories have motivated and broadened my perspective in life; my parents, whose love and support have guided me through every stage of my life; and my husband, whose unconditional love, patience, and support has allowed me to stay optimistic in every situation.

TABLE OF CONTENTS

| | |
|---|----|
| Chapter 1 | 1 |
| Introduction | 1 |
| Chapter 2 Background | 4 |
| 2.1 Additive Manufacturing | 4 |
| 2.1.1 Printed Electronics | 6 |
| 2.2 Aerosol Jet Printing | 8 |
| 2.2.1 Physical process involved in AJP | 10 |
| 2.2.2 Focusing Ratio | 11 |
| 2.2.3 Software used in AJP | 12 |
| 2.2.4 Silver and its uses | 13 |
| 2.3 Screen Printing | 13 |
| 2.3.1 Copper paste | 15 |
| 2.4 Printed Circuit Board (PCB) Fabrication | 16 |
| 2.5 Ansys HFSS | 16 |
| 2.6 FR-4 Paper | 18 |
| 2.7 KEYENCE Microscope | 18 |
| 2.8 VNA (Vector Network Analyzer) | 19 |
| 2.9 Return Loss | 20 |
| 2.10 Microwave Frequency Band | 21 |
| Chapter 3 | 22 |
| Design, Experiment and Methodology | 22 |
| 3.1 Antenna Design and Geometry | 22 |
| 3.2 Aerosol Jet Printing – Materials and Method Used | 24 |
| 3.2.1 Conversion of DXF File to G-code | 24 |
| 3.2.2 Ink Preparation | 25 |
| 3.2.3 Optimized parameters for the printing process | 25 |
| 3.2.4 Setting the atomizer voltage | 25 |
| 3.2.5 Printing Method | 26 |
| 3.2.6 Post-processing method for AJP | 27 |
| 3.3 Screen Printing – Materials and Method Used | 29 |
| 3.3.1 Necessary supplies | 30 |
| 3.3.2 Steps involved in the screen printing method | 30 |

| | |
|---|----|
| 3.3.3 Post processing method for screen printing | 31 |
| 3.4 PCB Fabrication – Method Used..... | 32 |
| 3.4.1 PCB Design Layout Process | 33 |
| Chapter 4 | 34 |
| Results and Discussion..... | 34 |
| 4.1 Antenna fabrication using AJP and Screen Printing | 34 |
| 4.2 Antenna Measurement | 36 |
| 4.2.1 Reflection Coefficient..... | 36 |
| 4.2.2 Radiation Pattern and 3D Polar Plot | 44 |
| 4.2.3 Reference Comparison Table..... | 47 |
| Chapter 5 | 49 |
| 5.1 Summary and Conclusion | 49 |
| 5.2 Future Work..... | 50 |
| References..... | 51 |
| Appendix..... | 55 |

LIST OF FIGURES

| | |
|---|----|
| Figure 1. Different phase involved in AM process [16] | 5 |
| Figure 2. Steps of electronics printing | 7 |
| Figure 3. Classification of printing process | 8 |
| Figure 4. Computational fluid dynamics model showing how different aerodynamics lenses are used to collimate a polydisperse aerosol stream [27] | 9 |
| Figure 5. Physical process involved in aerosol jet printing | 10 |
| Figure 6. Ultrasonic atomization process..... | 11 |
| Figure 7. Flow Vision software showing sheath flow rate and atomizer flow rate | 12 |
| Figure 8. FlashCut CNC with G-code..... | 13 |
| Figure 9. Schematic of screen printing | 15 |
| Figure 10. Copprint copper paste LF-350 [36] | 16 |
| Figure 11. Keyence Microscope 7000 series [41] | 19 |
| Figure 12. Keysight E5080B ENA VNA [43]..... | 20 |
| Figure 13. Four different antenna design (a) Design-1 (b) Design-2 (c) Design-3 (d) Design-4 simulated using Ansys HFSS..... | 22 |
| Figure 14. Experimental set-up for aerosol jet printing..... | 24 |
| Figure 15. Mist coming out from the aerosol port | 26 |
| Figure 16. Images showing profile of the NanoJet print head (a) with the ink cartridge and flow cell installed and (b) the ink cartridge and flow cell removed [27] | 27 |
| Figure 17. (a) Post-processing method using degassed vacuum chamber for aerosol printed antenna and (b) Printed antenna in a flexible substrate | 28 |
| Figure 18. Antenna measurement on Keysight E5080B ENA VNA..... | 28 |
| Figure 19. Breakdown of steps included in aerosol jet printing | 29 |
| Figure 20. Experimental set up for screen printing..... | 29 |
| Figure 21. Process for the printing of antenna design | 31 |
| Figure 22. Post-processing method for screen printed antenna using laminator | 32 |
| Figure 23. Design layout in GerbView | 33 |
| Figure 24. Four antenna design fabricated using aerosol jet printing..... | 34 |
| Figure 25. Four antenna design fabricated using screen printing | 35 |
| Figure 26. Factory manufactured antenna on a PCB Board | 35 |
| Figure 27. Measurement of the depth of conductive part using (a) AJP and (b) screen printing. | 36 |
| Figure 28. The PCB fabricated, simulated, screen printed and AJP reflection coefficient of antenna design 1 | 37 |
| Figure 29. Reflection coefficient of (a) AJP, (b) Screen Printing, (c) Simulation, and (d) PCB fabrication of antenna design 1 | 38 |
| Figure 30. The PCB fabricated, simulated, screen printed and AJP reflection coefficient of antenna design 2..... | 38 |
| Figure 31. Reflection coefficient of (a) AJP, (b) Screen printing, (c) Simulation, and (d) PCB fabrication of antenna design 2 | 39 |
| Figure 32. The PCB fabricated, simulated, screen printed and AJP reflection coefficient of antenna design 3..... | 40 |
| Figure 33. Reflection coefficient of (a) AJP, (b) Screen Printing, (c) Simulation, and (d) PCB fabrication of antenna design 3 | 41 |

| | |
|---|----|
| Figure 34. The PCB fabricated, simulated, screen printed and AJP reflection coefficient of antenna design 4..... | 41 |
| Figure 35. Reflection coefficient of (a) AJP, (b) Screen Printing, (c) Simulation, and (d) PCB fabrication of antenna design 4..... | 42 |
| Figure36. Radiation pattern and 3D Polar Plot for Design 1..... | 45 |
| Figure 37. Radiation pattern and 3D Polar Plot for Design 2..... | 45 |
| Figure 38. Radiation pattern and 3D Polar Plot for Design 3..... | 46 |
| Figure 39. Radiation pattern and 3D Polar Plot for Design 4..... | 46 |

LIST OF TABLES

| | |
|--|----|
| Table 1. Different microwave frequency range according to letter designation..... | 21 |
| Table 2. Parameters considered to design antenna | 23 |
| Table 3. Optimized parameter used in AJP | 25 |
| Table 4. Center frequency and it's corresponding bandwidth and S11 parameters..... | 43 |
| Table 5. Comparison of referenced antenna | 47 |

LIST OF ABBREVIATIONS

ACS: Asymmetric Coupled Stripline
AJP: Aerosol Jet Printing
AM: Additive Manufacturing
CAD: Computer Aided Design
CNC: Computer numerical control
dB: Decibel
DUT: Device Under Test
DXF: Drawing Exchange Format
EM: Electromagnetic
FEM: Finite Element Method
FR4: Flame Retardant 4
HFSS: High Frequency Structural Simulator
IDS: Integrated Deposition Solutions
IEEE: Institute of Electrical and Electronics Engineers
ITU: International Telecommunication Union
LCD: Liquid-crystal display
NATO: North Atlantic Treaty Organization
OLED: Organic light-emitting diodes
PCB: Printed Circuit Board
PE: Printed Electronics
RF: Radio Frequency
SCCM: Standard cubic centimeters per minute
SMA: Sub Miniature Version A
STL: Standard Tessellation Language
TLC: Thermal Laminating Company
UWB: Ultra-wideband
VNA: Vector Network Analyzer

Chapter 1

Introduction

In recent years, additive manufacturing (AM) has become an interesting approach for fabricating printed electronics because of its capacity to build complicated shapes with great precision. The commercial usage of AM dates back to 1987, when 3D systems introduced stereolithography (SL), a technology that uses a laser to solidify thin layers of ultraviolet (UV) light-sensitive liquid polymer [1]. Since then, different manufacturing methods such as material extrusion, sheet lamination, direct energy deposition, material jetting, binder jetting [2] have been introduced in the industry based on different types of applications. Many researchers have contributed to the study of the printing capabilities, electrical characteristics, procedures for synthesis of fundamental nature of the metallic, organic, and inorganic nanomaterials [3]. The ability to create smart electronics devices and circuits on flexible and rigid substrate using additive manufacturing process is one development that inspired an entire printed electronics industry. Commonly used electronic components such as transistors, sensors and displays have been printed using AM methods. Printed electronics have numerous benefits compared to conventional electronics production processes, such as cheaper prices, more design flexibility, and the ability to print on a wide range of substrates that include ceramics, metals, thermoplastics. Various application areas in the medical field, wireless communication systems, and aerospace use printed electronic devices such as sensors, actuators, and antennas that need to be structured properly to achieve suitable mechanical and electrical performance. Inflexibility due to form factor and weight considerations has always been one of the main impediments to technical improvements of next-generation IoT connected devices [4]. However, advances in engineered materials have been used to improve

flexible electronics. Flexible electronic devices are more likely to be lightweight, portable, less costly, less harmful to the environment, and biodegradable [5].

Today, with information being shared wirelessly, it is essential for the flexible electronics industry to integrate flexible antennas operating in desired frequency bands. The demand for flexible wireless devices has been increased tremendously in health-monitoring systems and daily-life wireless devices. This trend is also driven by the increasing popularity of portable devices like digital watches, cell phones, eyewear devices.

Since flexible antenna unlike rigid antennas can be integrated with or worn on the body in the form of accessories, there is a growing number of potential biomedical applications where microwave antennas are specifically used. Some of the widely used applications are in the detection of breast cancer [6], bone fractures [7], chemotherapy [8], hemorrhages [9], heart failure detection [10], continuous glucose monitoring [11]. Microwaves have an advantage over other methods like chemotherapy and imaging due to their non-ionizing radiation and non-invasive application, allowing for longer-term exposure to the human body without causing harm [12]. In contrast, X-ray exposure can be fatal to the human body, making microwave systems a safer option if practical limits are followed. With microwave systems, longer-term exposure can result in improved imaging while still ensuring the preservation of the tissues. Microstrip antennas, commonly in biomedical applications, were used in this study because of their low profile, light weight, and simplicity of integration with other components. Moreover, they are compatible with flexible substrates, making them appropriate for wearable sensors and implantable devices.

In this research, four different asymmetric coupled-stripline (ACS) fed microstrip antenna is designed, simulated in Ansys HFSS, and fabricated using two additive manufacturing methods, AJP and screen printing.

Objective of the research:

1. To design a flexible, and functional antenna.
2. To fabricate antenna using additive manufacturing process.
3. To understand the influence of different parameters used in aerosol jet printing.
4. To compare the results of contact printing and non-contact printing.
5. To evaluate the performance of antenna based on reflection coefficient.

Organization of the research:

This thesis is organized into 5 chapters. The first chapter describes the introduction of the study in additive manufacturing process. The second chapter focuses on the techniques and the process used in the work. The third chapter explains the methodologies and the experiment performed. The fourth chapter details on the results and discussion of the research. The fifth chapter discusses about the future work and concludes the thesis.

Chapter 2

Background

This chapter covers all the techniques and terminology used in the research. The basic principle involved in aerosol jet printing and screen printing are explained in detail along with the introduction of the software used to design the antenna. The KEYENCE model microscope and Keysight model VNA are also introduced as they were used to study the image of fabricated antenna design and measurement of antenna respectively.

2.1 Additive Manufacturing

Additive manufacturing (AM), known popularly as 3D printing, is a process of adding layer upon layer of material (ceramics, metals, or plastics) to create an object. The process starts with converting a design from any professional CAD software to the STL file format and manipulating the file for the specific machine setup requirement, building the parts, and following up with the post-processing method as shown in figure 1. Compared to conventional manufacturing methods, additive manufacturing processes have several benefits such as design freedom, versatility, optimization of the parts, and increased resource efficiency [13]. Over a time, names like rapid prototyping [14], layer-based manufacturing or, solid freedom fabrication have given way to AM for defining the overall manufacturing process. AM can generate intricate patterns and geometries that might be challenging to make using other techniques. It makes productive use of raw materials and creates minimal waste while maintaining satisfactory geometric accuracy [14], [15]. The main features that help AM stand out from the traditional manufacturing processes are the type of materials that can be used with AM, high-speed CNC machining, and the resolution of the design.

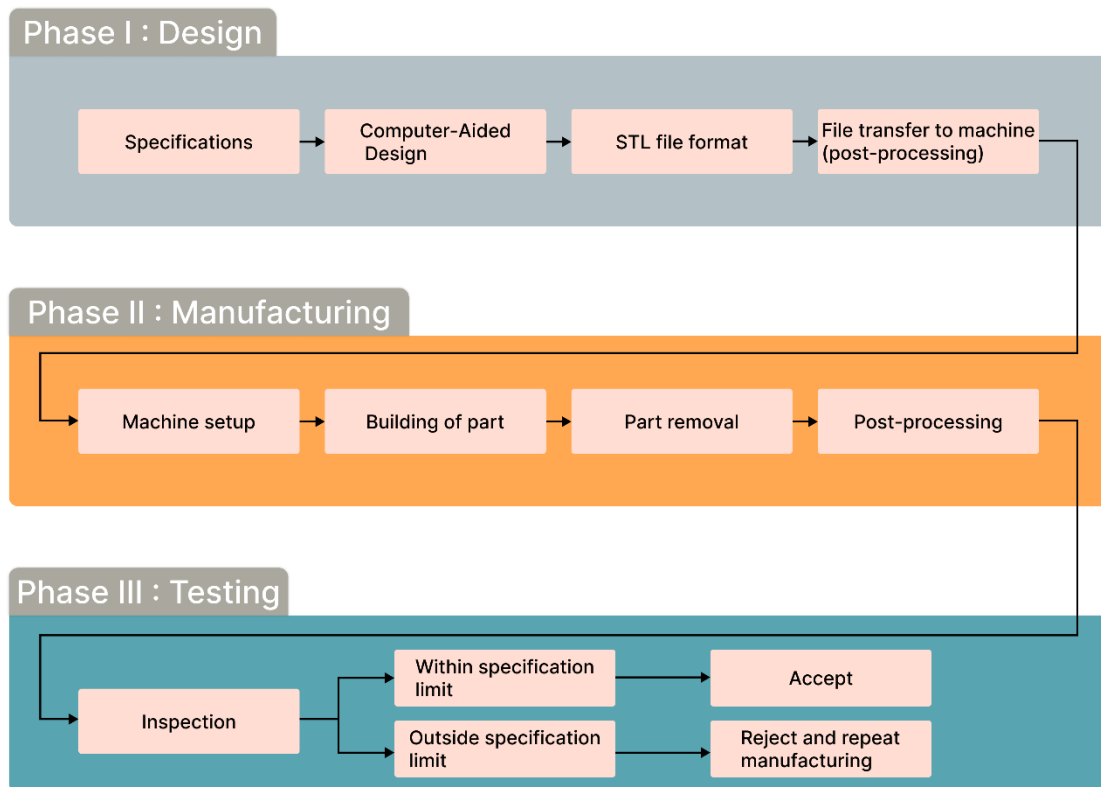


Figure 1. Different phase involved in AM process [16]

Different manufacturing methods based on different principles of application and uses are employed in industry. Examples include selective laser melting (SLM), fused deposition modelling (FDM), selective laser sintering (SLS), which is generally used to melt or soften the materials to create the layers, and stereolithography (SLA) which cures liquid materials [17].

2.1.1 Printed Electronics

The methods of printed electronics (PE) are used to fabricate electronic devices and circuits. This is a combination of text or graphic printing and electronic fabrication that allow the production of standard electronic devices/circuits which are eco-friendly, wearable, flexible, and lightweight [18]. PE is a growing field for functional nanomaterials, with applications ranging from flexible circuits and displays to electronics packaging and environmental and biomedical sensors. It is possible for printed electronics to provide sustainable and bio-degradable solutions which can reduce the amount of electronics waste produced by a growing amount of disposable electronics [19], [20].

Researchers have demonstrated printed electronic components which are passive, active and sensor. Active components use the nonlinear behavior of printed materials, and sensors are built based on the electro-mechanical characteristics of the printed structures, whereas passive components are designed and made based on electromagnetic properties of printed materials and shapes [21]. Antennas, RFID tags, gas sensor, temperature sensor, humidity sensor, color displays, OLEDs have been fabricated on a thin and flexible substrate [22], [23].

Three main steps included in printed electronics are: 1) Material selection, 2) The printing process, and 3) The post-printing process as shown in figure 2.

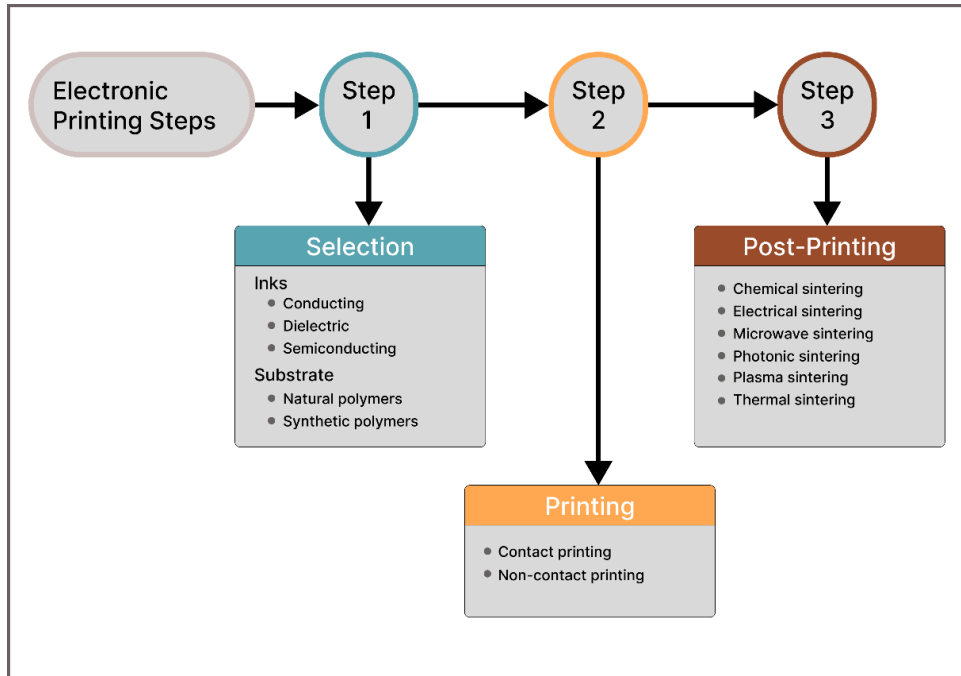


Figure 2. Steps of electronics printing

Different substrates and inks are chosen wisely based on the printing process used. The printing processes are further classified into contact printing and non-contact printing as shown in figure 3. In contact printing, the ink is in direct contact with the substrate. In non-contact printing, the ink is deposited onto the substrate through a nozzle. The selection of ink, the printing process, and the post-processing method are carried out based on the material used.

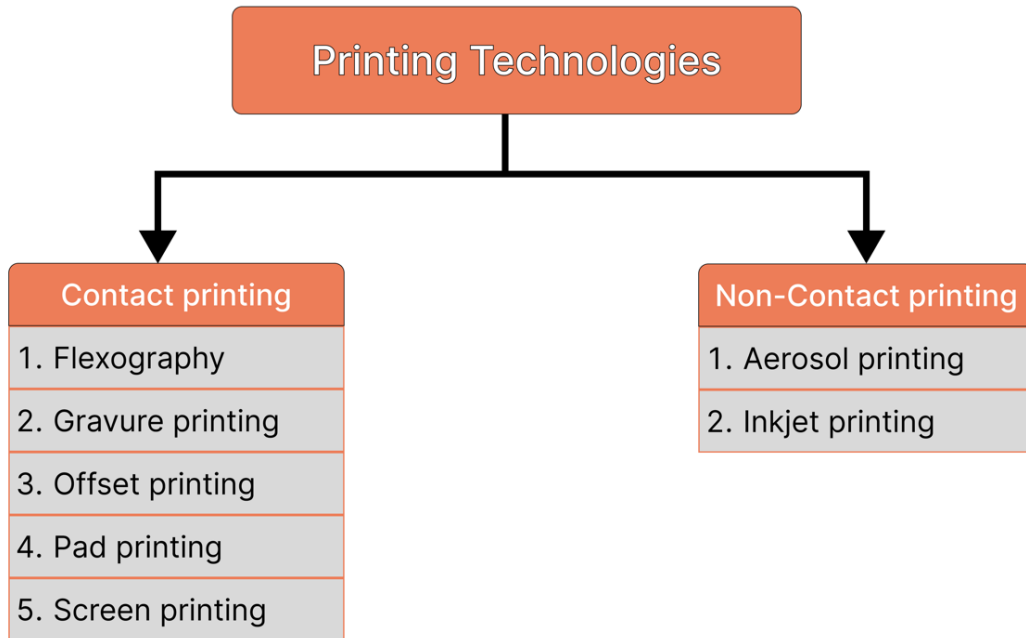


Figure 3. Classification of printing process

Printed electronics offer various advantages compared to the traditional manufacturing techniques. Some of the advantages were categorized by Kunnari et al. in terms of eco-design, which includes efficient material use, reduced use of hazardous compounds, and lower energy consumption during both the manufacturing and use phases [24]. The printed electronic devices also have advantageous physical properties, such as low weight, ability to stretch, and resistance to folding or bending, which are not achievable using traditional electronics [25]. Different printed electronic components can be found in everyday usage in radio frequency (RF) components, sensors, energy harvesting and storage, displays and many others.

2.2 Aerosol Jet Printing

Aerosol jet printing (AJP) which is under the umbrella of additive manufacturing has lately emerged as a potential manufacturing process for a wide variety of applications. It is a type of 3D

printing technology that uses a high-velocity jet of particles to deposit material on a substrate. It is commonly used to create micro-scale structures and patterns on a variety of materials, including metals, ceramics, and polymers. The technology can be used to print electronic devices, such as sensors and transistors, as well as other micro-scale structures, such as microfluidic devices and bio-medical implants.

There are different parameters that affect the deposition of the ink on the substrate, like sheath flow, aerosol flow, atomizer voltage, deposition nozzle size, and aerosol droplet size. Other parameters for the optimization of the deposition include print speed which can affect the thickness of the ink deposition, working distance between nozzle end and substrate, and platen temperature which can dry the ink on the substrate. AJP offers advantages that complement many existing approaches because of its non-contact, line-of-sight, and digital nature. The printing process accurately controls the location, geometry, thickness of the deposit and produces a smooth surface to ensure optimum antenna performance [26].

The NanoJet Desktop printer by Integrated Deposition Solutions (IDS) is employed to run the experiment for aerosol jet printing process. The basic collimation process is shown in figure 4.

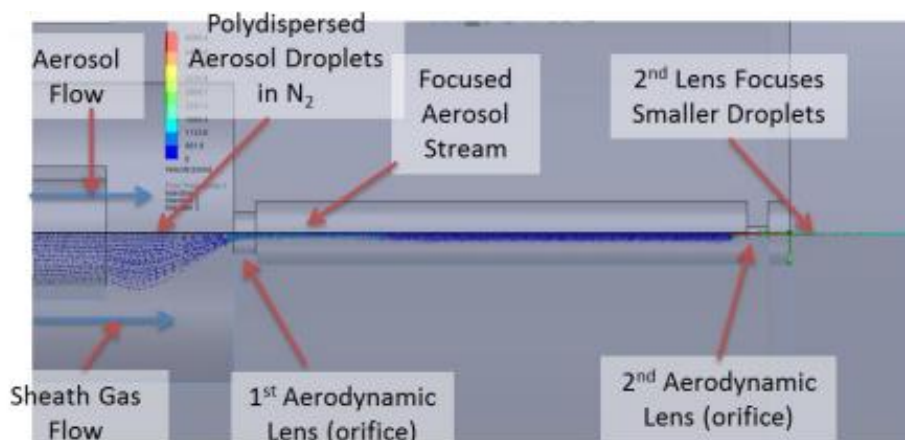


Figure 4. Computational fluid dynamics model showing how different aerodynamics lenses are used to collimate a polydisperse aerosol stream [27]

In the figure, the first gas stream is aerosol flow which contains aerosol droplets for the printing and the second gas stream is sheath flow which is used to concentrate the aerosol droplets into finely collimated beam that can be impressed onto a surface to produce a printed feature. The two gas streams merge and travel through a series of aerodynamic lenses, as depicted, to cause collimation [27].

2.2.1 Physical process involved in AJP

The physical process involved in the printing is shown in figure 5. The process begins in the aerosol chamber where the printing ink is stored. The functional nanoparticle is placed into the ink vial inside an atomizer. The ultrasonic transducer atomizes the ink into an aerosol where the atomization of the ink is controlled by atomizer voltage. The carrier, or atomizer gas flow, then carries this aerosol out of the vial and in the direction of the deposition head.

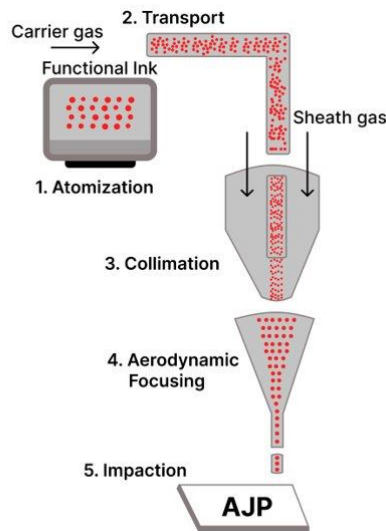


Figure 5. Physical process involved in aerosol jet printing

A carrier gas then aerosolizes a functional ink and delivers it to the substrate as shown in figure 6, achieving resolution as fine as 10 μm with speed easily reaching up to 200 mm/second. The sheath gas is introduced, surrounding aerosol to help it focus and prevent from clogging. Droplets are

aerodynamically focused as they pass through a deposition nozzle because of inertial effects in the narrow, nozzle's converging. The droplets are then released in an impinging jet in the direction of the substrate [26].

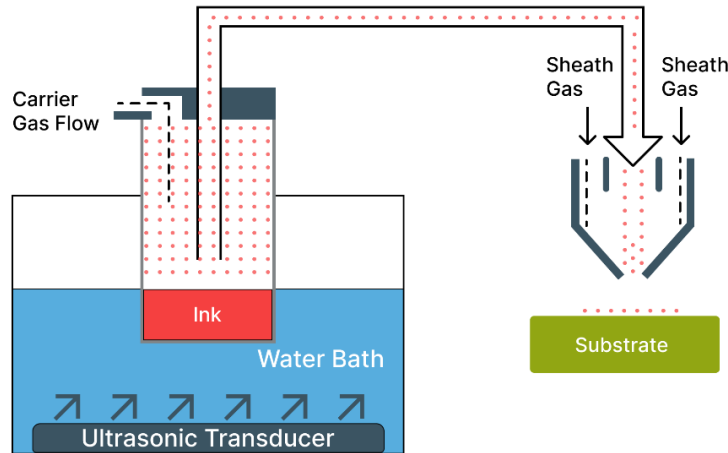


Figure 6. Ultrasonic atomization process

2.2.2 Focusing Ratio

The line geometry depends significantly on the focusing ratio. It is the relationship between the sheath gas flow rate and atomizer gas flow rate and is depicted as:

$$\text{Focusing ratio} = \frac{\text{Sheath Gas Flow Rate}}{\text{Atomizer Gas Flow Rate}}$$

As the sheath gas flow rate controls the deposition rate, it is recognized that the focusing ratio is essential for controlling the line features and resistance. The line deposited on the substrate depends on this ratio whether it prints a fine line or thick line on each pass. With a constant carrier gas flow rate and speed rate, the line width decreases, and the thickness increases as the sheath gas flow rate or focusing ratio increases. But the thickness of the line decreases with the increase of

speed rate [28]. Different parameters were optimized on this research to understand its effect to produce a high-resolution conductive line.

2.2.3 Software used in AJP

Two computer programs called Flow Vision and Flashcut CNC software were used to run the printing process. Flow Vision is used to control the flow of the sheath gas flow and atomizer gas flow. All the antenna designs were created on Ansys HFSS (High Frequency Structural Simulator). The generated DXF file from Ansys HFSS were used in Fusion 360 to create the G-code file. The G-code file then is loaded into the Flashcut CNC where the motion of printing is controlled. The G-code based controller allows end users to select an off-the-shelf CAM system to make print toolpaths for the nanojet printer.



Figure 7. Flow Vision software showing sheath flow rate and atomizer flow rate

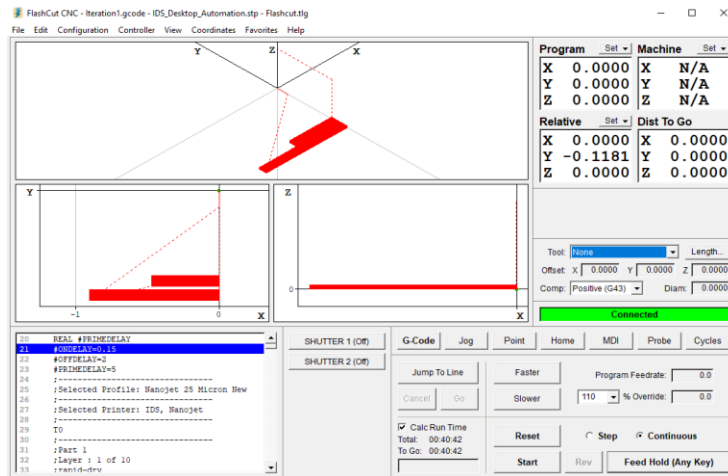


Figure 8. FlashCut CNC with G-code

2.2.4 Silver and its uses

The functional nano particles silver ink used in our research is from UTDots. UTDAg (UTDots Ag40X) is made up of silver nanoparticles with an average size of approx. 10 nm that are disseminated in a liquid carrier. Because of their stabilized surfaces, UTDAg inks are stable at room temperature and are readily soluble in nonpolar organic solvents [29]. Silver nanoparticles are highly conductive and have a high signal capacity. They have unique physical and chemical properties due to their small size and are used in a wide range of applications including medicine, electronics, and environmental remediation. In medicine, silver nanoparticles are used as antimicrobial agents which can make them useful in biomedical-related products such as implantation and wound dressings, while in electronics they are used as conductive agents in products such as computer hard drives and LCD screens [30].

2.3 Screen Printing

Screen Printing is a process for creating a picture or pattern where ink is pushed through a stencil or mesh which is made of plastic, steel, or metal fiber. The stencil, also referred to as a "screen,"

is made by blocking off areas of the mesh with a non-permeable material, leaving only the desired image or design visible. The fundamental components of screen printing are screen mesh, squeegee, substrate, paste, and base. The screen mesh contains the specific pattern through which the paste is passed and deposited onto the substrate. The squeegee helps to push the paste from the pores of the screen. The mechanical force that the squeeze exerts against the screen mesh makes it easier for the paste to ooze through open pores [31].

The general schematic of screen printing is shown in the figure 9. The substrate rests on top of the working base. The paste is swiped on the screen frame with the help of a squeegee. It is important to leave some distance between the screen frame and substrate to prevent the paste flooding under the stencil. This distance between the screen frame and the substrate is called snap-off. Drying of the paste depends on the ultraviolet (UV) curing, oxidation, or blowing air onto the deposition of paste on the substrate. The quality of deposition depends on the paste rheology, composition, texture, thickness of the screen, and snap-off distance.

The printing process involved in screen printing is considered simpler and less expensive than traditional fabrication methods like the vacuum deposition technique and photolithography [32]. The method is recognized as affordable, suitable for mass production, and easy to work with a wide range of substrate [33]. Once the initial setup is complete, printing products in large quantities is relatively rapid and simple, making it cost-effective. Studies have demonstrated screen printing to print electrodes, sensors, carbon electrode. The general schematic for Screen Printing is shown below.

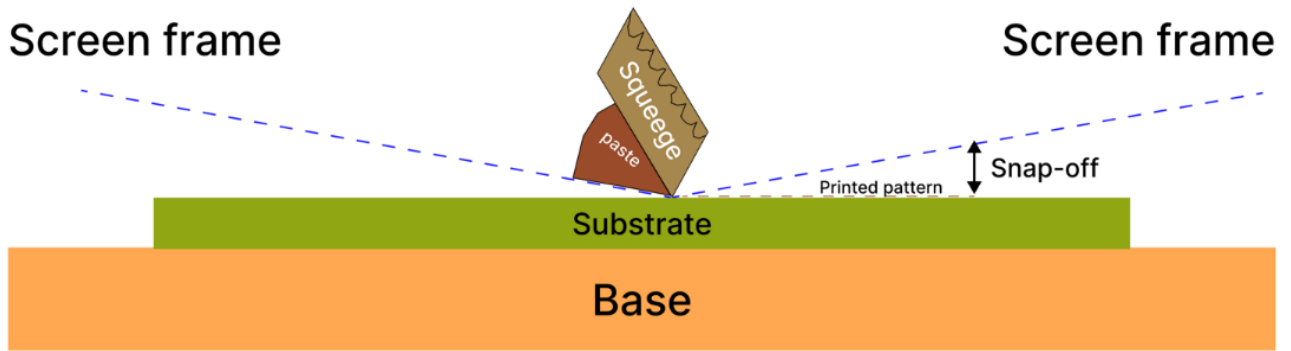


Figure 9. Schematic of screen printing

2.3.1 Copper paste

Copper paste is considered a plausible replacement for silver paste in the future due to the expense of silver nanoparticles [34]. This can be used in the application of flexible electronics where the paste is used as a conductor to connect the various components of the device and to transport electrical current. The paste is typically screen-printed onto a flexible substrate, such as a plastic or polymer film, in a pattern that corresponds to the electrical circuit of the device. The paste is then cured, typically through heating or UV exposure, to solidify the copper and create a conductive trace. It is required that the paste must have good adhesion to the substrate and must maintain its conductivity even when bent or folded.

There are some limitations to using copper paste since it is more prone to oxidation, which is why research is ongoing to improve the performance of copper paste used in flexible electronics, including development of new formulations of paste, new curing methods, and new substrate materials to improve the performance of the devices.

The copper paste used in this research is LF-350 from Copprint. With the inclusion of nano Copper particles, Copprint LF-350 offers oxidation-free, high conductivity, as well as quick self-sintering and curing at 200°C [35].



Figure 10. Copprint copper paste LF-350 [36]

2.4 Printed Circuit Board (PCB) Fabrication

Printed Circuit Boards (PCBs) are the foundation of all significant electronics. In simple language, a PCB is a circuit board that transmits electrical impulses among electronic devices to meet the board's electrical and mechanical circuit needs. To fabricate a PCB, a sheet of copper is typically layered over an insulating material. Excess (non-circuit forming) copper is then eliminated via etching, leaving behind the required circuit design. Different steps like design, etching, drilling, surface finish, soldering, profiling, and V-Scoring is also often involved in the fabrication of PCB board [37].

2.5 Ansys HFSS

Ansys HFSS (High-Frequency Structure Simulator) is a simulation software used to model and analyze the behavior of electromagnetic fields in high-frequency and high-speed devices such as antennas, microwave devices, and RF (radio frequency) circuits [38]. It uses the finite element

method (FEM) to solve Maxwell's equations, which govern the behavior of electromagnetic fields.

HFSS can be used to simulate a wide range of devices and systems, including:

- 3D electromagnetic (EM) simulations for antenna design and analysis
- EM-circuit co-simulation for RF and microwave devices
- EM-thermal analysis for power amplifiers
- EM-structural analysis for antenna-structure interactions
- EM-circuit-thermal analysis for power amplifiers and RF components
- EM-circuit-structural analysis for antenna-structure-circuit interactions

HFSS has a graphical user interface and a scripting interface, which makes it user-friendly and allows for automation and parametric studies. It also supports various types of simulation methods such as frequency domain, time domain, and harmonic balance.

The software simulates and evaluates the design based on the desired goals. The radiation pattern, S-parameter plot, movement, fatigue, fractures, fluid flow, temperature distribution, electromagnetic efficiency, and other effects over time can be generated from the software [39]. Once the simulation is done, the design is exported for the fabrication process. The AutoCAD DXF file is one of the most common exported file formats. To export the design, the model is extracted along the XY plane. Each component of the model is extracted and saved separately in a DXF format. The components are then imported back into the Ansys HFSS software in their DXF formats, combined by placing each exported layer on the other, and then exported as one file. The final exported formats depend on the fabrication company's requirements. All the design simulation in this research is done via Ansys HFSS.

2.6 FR-4 Paper

The dielectric material used in printed circuit boards which is frequently used is FR-4. The "FR" represents for flame retardant, while the "4" represents for woven glass-reinforced epoxy resin. The FR-4 dielectric constant varies from 3.8 to 4.8 based on the type of glass weave, thickness, and the resin content. It is used in a wide range of electronic devices, from small consumer electronics to large industrial systems. While the specific properties of FR-4 may differ among the manufacturers, the different advantages of FR-4 materials include low-cost material, high dielectric strength, ability to bear mechanical load, resistance to moisture, higher glass transition temperature, and higher decomposition value [40].

The flexible FR-4 paper used in our research is HF FR4 sheet from Kunshanshi Honglei Electronics Technology Co. Ltd. which has a thickness of 0.1 mm.

2.7 KEYENCE Microscope

The KEYENCE microscopes are well-known for their high-resolution imaging and advanced measurement capabilities, and they are used in a variety of industries including electronics, semiconductors, and biotechnology. The Keyence Microscope VHX-S750E was used in our research to take all the magnified images of the samples. The user only needs to position the target on the stage; alignment, focus adjustment, magnification switching, and other tasks are all totally automatic after that. Even beginner users can perform observation on the specified area precisely and stress-free. A wide range of measurements, such as distance between two points, angle, diameter, parallel lines, area, and so on, can be performed on the screen in real-time using simple mouse operations. The microscope also offers High-speed image stitching which is six times more data than the conventional systems [41]. Different lenses like VHX-E20, VHX-E100, and VHX-E500 lenses were used to study and capture the images.



Figure 11. Keyence Microscope 7000 series [41]

2.8 VNA (Vector Network Analyzer)

A Vector Network Analyzer (VNA) is used to measure the electrical characteristics of RF and microwave devices, such as filters, amplifiers, and antennas. During the design and manufacturing processes, network analyzers are the main instrument for measuring transmission, reflection, and impedance, as well as s-parameters. The VNA has two main components, a signal generator and a receiver, which are connected to the device under test (DUT). The signal generator sends the RF signal to the DUT, and the receiver measures the signal that is returned. By measuring the difference between the input and output signals, the VNA can determine the device's transmission characteristics (transmission coefficient, insertion loss, gain), reflection characteristics (reflection coefficient, VSWR, return loss) and s-parameters S_{11} , S_{12} , S_{21} , S_{22} [42].



Figure 12. Keysight E5080B ENA VNA [43]

2.9 Return Loss

Return loss is a measure of the amount of energy that is reflected back to the source when a signal is transmitted down a transmission line. It is often expressed as a negative number and is measured in dB. A higher return loss number means that the signal is more effective because less energy is being reflected back to the source. A lower return loss value indicates that more energy is being reflected back, and the signal is less efficient. Return loss is crucial because reflected signals can distort and impair the overall signal quality of the originating transmission. To lower the amount of distortion and enhance the signal quality, high return loss is preferred. The transmission line impedance, the load impedance, and the signal reflection coefficient are all variables that might have an impact on return loss. Return loss is widely used to assess the signal's quality and the functionality of various components (such as power amplifiers, filters, and antennas) connected to the transmission line.

2.10 Microwave Frequency Band

The microwave frequency range spans from 1 GHz to over 100 GHz and is categorized into various letter bands by organizations such as IEEE Radar Bands, NATO Radio Bands, and ITU Bands [44]. These various sub-bands according to letter designation are shown below.

Table 1. Different microwave frequency range according to letter designation

| S.N. | Letter Designation | Frequency Range |
|------|--------------------|--------------------|
| 1 | L-band | 1 GHz to 2 GHz |
| 2 | S-band | 2 GHz to 4 GHz |
| 3 | C-band | 4 GHz to 8 GHz |
| 4 | X-band | 8 GHz to 12 GHz |
| 5 | Ku-band | 12 GHz to 18 GHz |
| 6 | K-band | 18 GHz to 26.5 GHz |
| 7 | Ka-band | 26.5 GHz to 40 GHz |
| 8 | V-band | 40 GHz to 75 GHz |
| 9 | W-band | 75 GHz to 110 GHz |
| 10 | mm-wave band | 110 GHz to 300 GHz |

The different frequency bands are used in different applications based on the requirements which are later explain in this thesis. The design model of antenna, experimental set-up and the methods are explained in the next chapter.

Chapter 3

Design, Experiment and Methodology

For our study, we choose one non-contact printing method which is aerosol jet printing (AJP) and one contact printing method which is screen printing. This chapter explains the design of the antennas, experimental setup and the post-processing method involved in the printing process.

3.1 Antenna Design and Geometry

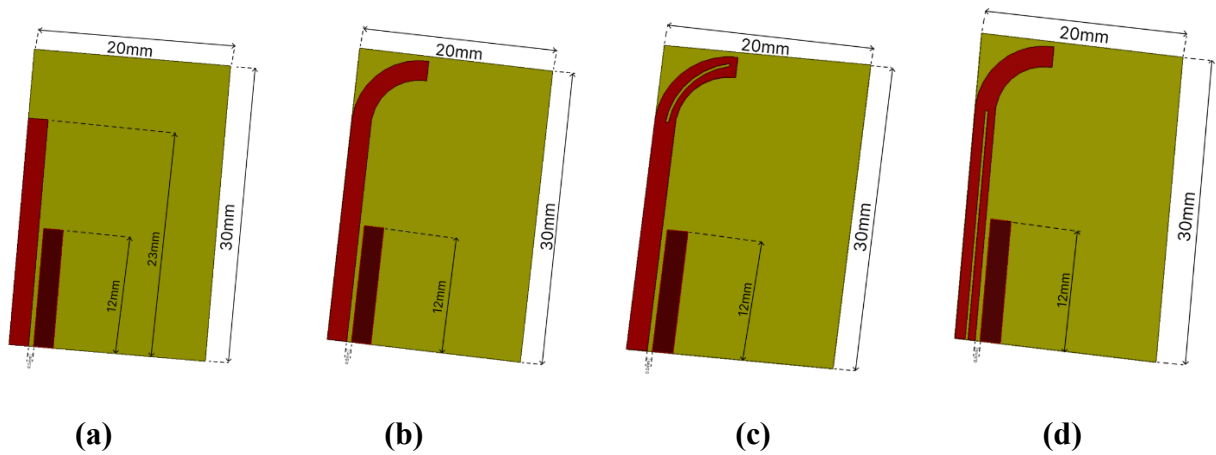


Figure 13. Four different antenna design (a) Design-1 (b) Design-2 (c) Design-3 (d) Design-4 simulated using Ansys HFSS

Four different microstrip antenna designs using same dielectric substrate are shown in figure 13. The designs comprise of a radiating patch, a ground plane and a feeding point. The substrate material is flexible FR-4 since this can enable a wider range of applications in the bio-medical field and wearable sensors. The substrate thickness was chosen to be 0.1 mm for all the antenna designs to evaluate a performance comparison of the proposed designs. The patch is chosen copper for it to be conductive material. Considerations such as biocompatibility, polarization, and choice of materials were also factored into designing the antenna. Important design parameters considered are shown in table 2.

Table 2. Parameters considered to design antennas

| S.N. | Parameters | Specifications |
|------|------------------------|------------------------|
| 1 | Operating Frequency | 1-20 GHz |
| 2 | Dielectric substrate | FR4 |
| 3 | Dielectric constant | 3.55 |
| 4 | Thickness of substrate | 0.1 mm |
| 5 | Feeding technique | Asymmetric-Coupled fed |
| 6 | Substrate size | 30 mm x 20 mm |
| 7 | Input Impedance | 50 Ω |
| 8 | Height of conductor | 0.1 mm |

Simulation of the antenna was performed using Ansys High Frequency Structural Simulator (HFSS) Electronics Desktop v.20. All four antennas have the FR-4 substrate dimension of 30 x 20 x 0.1 mm³. All these designs have a radiating patch and a ground plane which are separated by 0.5 mm. For the first design, top stripline is 23 mm x 2 mm and its asymmetric stripline is 12 mm x 2 mm. For the remaining three designs, the top stripline is 33 mm x 2 mm and its asymmetric stripline is 12 mm x 2 mm as well. For measurement data, a 50-ohm coaxial probe feed is used for excitation. After analyzing all the simulation results, the DXF file was extracted from the Ansys HFSS to proceed with fabrication.

3.2 Aerosol Jet Printing – Materials and Method Used

The experimental set-up using Aerosol Jet Printing method is shown in the figure 14.

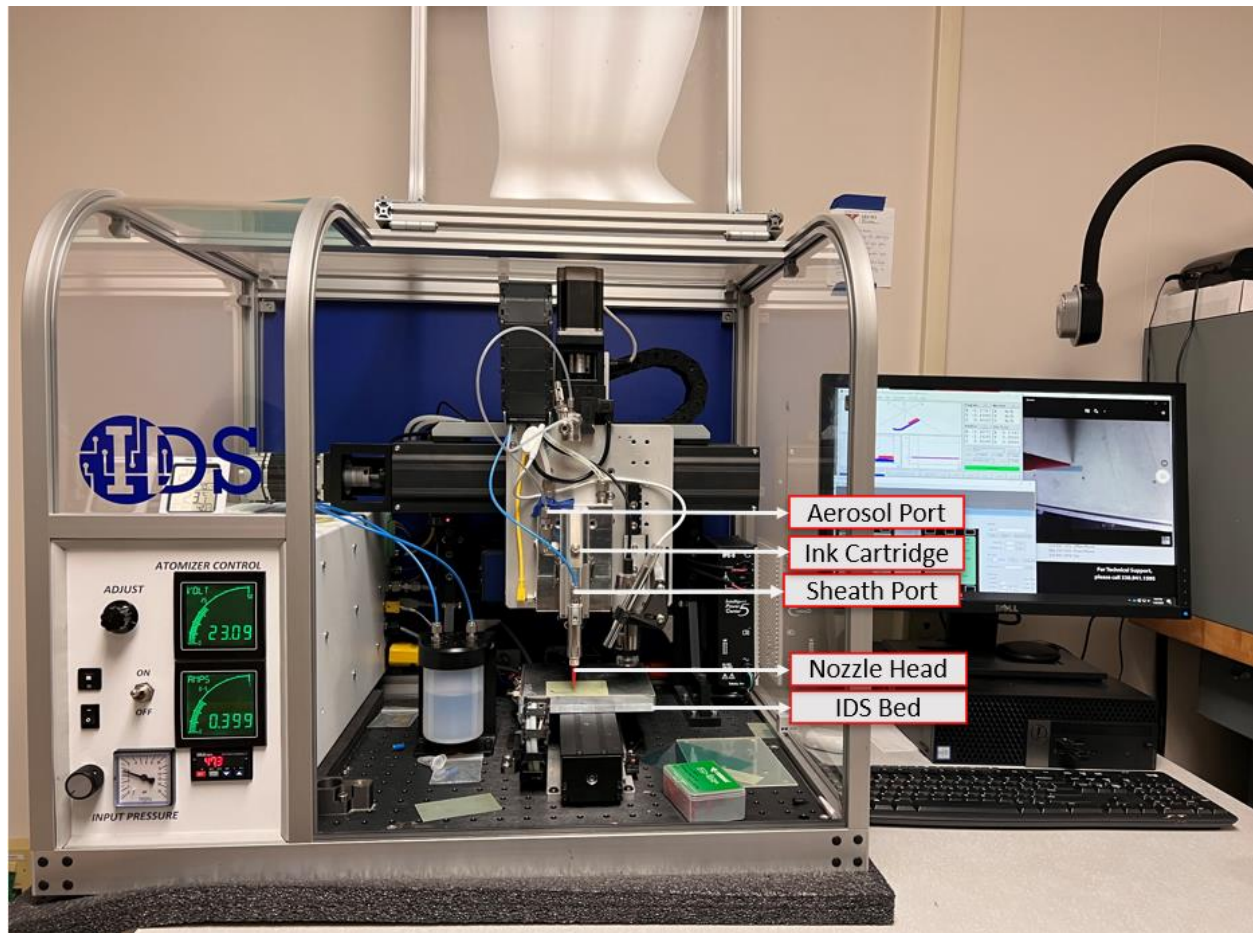


Figure 14. Experimental set-up for aerosol jet printing

3.2.1 Conversion of DXF File to G-code

All the antenna designs were created and simulated in Ansys HFSS. After running the final simulation, the files were extracted in DXF format/extension. Only the conductive parts were extracted in the DXF file and loaded into the Fusion 360 to convert it to the G-code. Different settings like print speed, and layers of the printing were optimized while creating G-code. After making the necessary changes to the setting, the files were converted to G-code format since the Flashcut CNC software accepts G-code files.

3.2.2 Ink Preparation

All the experiments related to aerosol jet printing were carried out with nanoparticle silver ink (UTDAg40X). The silver ink is suitable for the aerosol jet printer's ultrasonic atomizer, which has a preferred ink viscosity range of 1-5 cP [28]. For each printing in our experiment, 500 microliters of the ink were mixed with 75 microliters of terpineol which acts as a cosolvent.

3.2.3 Optimized parameters for the printing process

Since various parameters such as sheath flow, aerosol flow, atomizer voltage, and platen temperature play a vital role in the final result of the print, several tests were run to get the fine deposition of the aerosol. Table 3 demonstrate the utilized value for the experiments.

Table 3. Optimized parameter used in AJP

| Parameters | Value |
|----------------------|-------------|
| Sheath Gas Flow | 55-65 SCCM |
| Atomizer Gas Flow | 6-8 SCCM |
| Atomizer Voltage | 23 V |
| Platen Temperature | 60°C |
| Printing nozzle size | 250 μ m |

3.2.4 Setting the atomizer voltage

Since there are two gas stream- atomizer and sheath gas flow, it is important to verify the aerosol mist coming out from the aerosol port before we start the printing process. We checked this mist to make sure that our ink has been atomized properly. To do so, a computer program called Flow Vision is used, where we can control the sheath gas flow and atomizer gas flow. To start, we set

the sheath gas flow was set at 40 SCCM and the atomizer voltage was set at 0V. The atomizer voltage was then adjusted until there was good flow of mist coming out from the atomizer port. That atomizer voltage worked out to be 23 V which was then used as a fixed atomizer voltage to run the print.

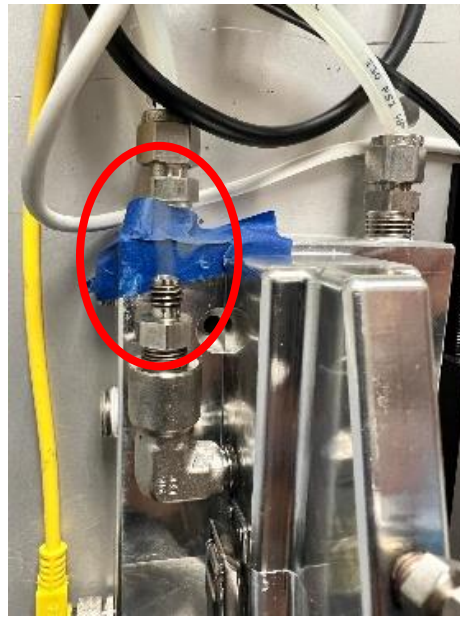


Figure 15. Mist coming out from the aerosol port

3.2.5 Printing Method

The FR-4 substrate used in our experiment was placed on the bed of the printer. The bed, also called the platen, was maintained at 60°C temperature throughout the printing process. The prepared ink was put inside the ink vial of the ink cartridge. It was then attached to the atomizer base as shown in figure 16.

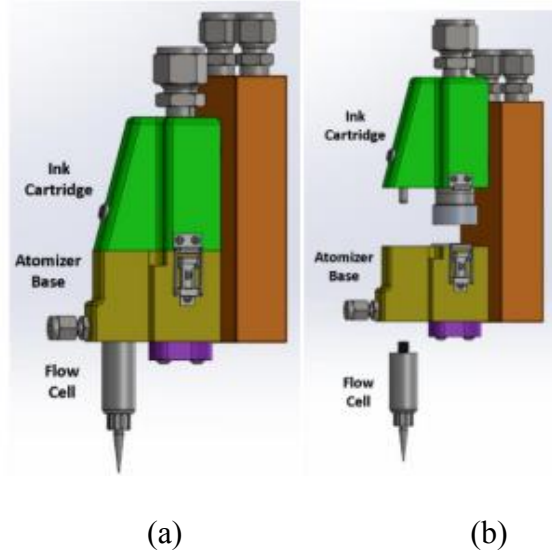


Figure 16. Images showing profile of the NanoJet print head (a) with the ink cartridge and flow cell installed and (b) the ink cartridge and flow cell removed [27]

The atomizer base was filled with 16 ml of distilled water to ensure the proper atomization of the ink inside the ink cartridge. The amount of ultrasonic energy that can be coupled to the ink cartridge will be reduced if the water level is not sufficient [27]. After all the settings were made, the printing process could be carried out.

3.2.6 Post-processing method for AJP

After the successful deposition of the aerosol onto the substrate, the next step was to make the deposition conductive. For that, the samples were cured using a fisher brand degassed vacuum chamber shown in figure 17 (a). At first, the samples were cured at 80°C for 30 minutes. Then the temperature was increased to 250°C for another 30 minutes. The samples were left inside the vacuum chamber for the next 1 hour. It was then tested for conductivity and the antenna measurement were done using VNA as shown in figure 18.



(a)



(b)

Figure 17. (a) Post-processing method using degassed vacuum chamber for aerosol printed antenna and (b) Printed antenna in a flexible substrate

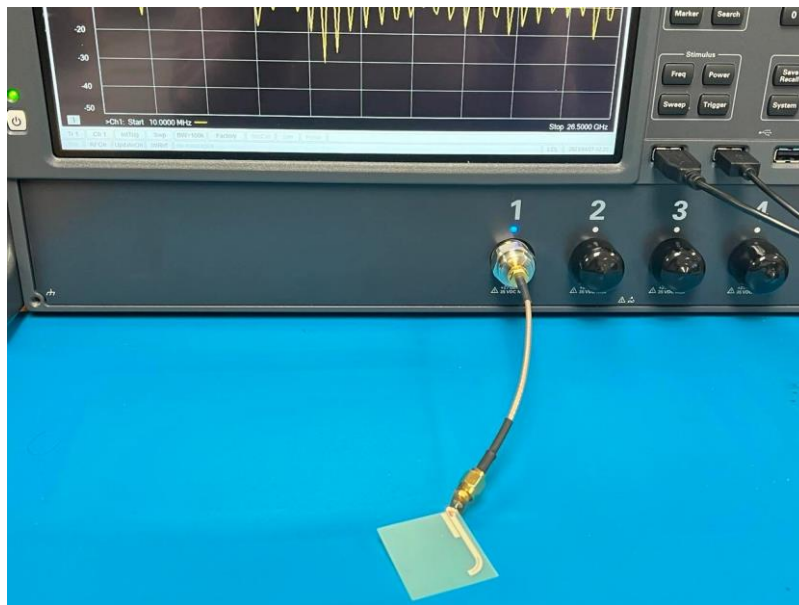


Figure 18. Antenna measurement on Keysight E5080B ENA VNA

The step-by-step procedure included in an aerosol jet printing method is shown in the figure 19.

Aerosol Printed Asymmetric Coupled Stripline (ACS) fed Microstrip Antenna for Biomedical Applications

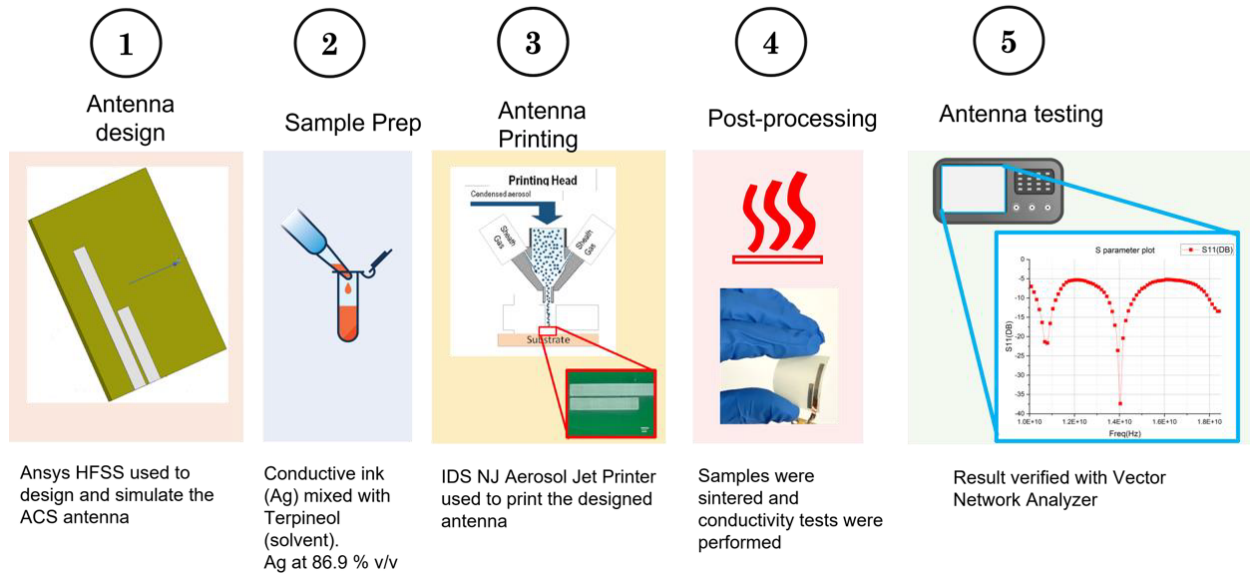


Figure 19. Breakdown of steps included in aerosol jet printing

3.3 Screen Printing – Materials and Method Used

The experimental set-up using screen printing is shown in the figure 20.

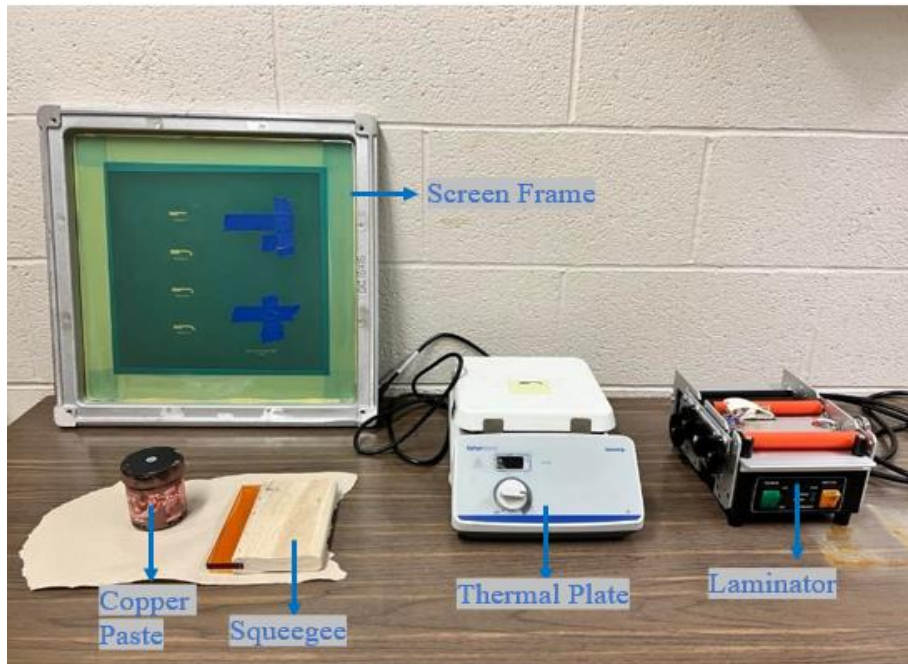


Figure 20. Experimental set up for screen printing

3.3.1 Necessary supplies

To work with screen printing process, we first started with the necessary supplies to carry out the process which include screen frame, paste, squeegee, and equipment to run the drying process and the sintering process. The Screen frames used for the research were from NBC Meshtec. The frame size is 15 x 15 inches inside which all the antenna designs were incorporated. It is a polyester screen 280 mesh per inch with 35-micron thread diameter. The emulsion thickness set was 15+/-2 micron. The copper paste (LF-350) used in the research was from Copprint. This specific paste is known for its excellent printability, high conductivity, nano copper particle size for pattern precision, and environment friendliness [36]. The paste was stored in a sealed container at -10°C in a refrigerator. All the tests were run on a flexible FR-4 substrate. As a part of post-processing, we used the fisher brand thermal plate for the drying process and TLC Laminator for the sintering.

3.3.2 Steps involved in the screen printing method

The FR-4 substrate was placed on top of the workbench which acted as a base. The screen frame is placed above the FR4 paper. The snap-off distance was then created between the screen frame and FR4 paper where the screen frame was tilted at a certain angle to avoid the excess paste oozing out from the mesh. At this time, the copper paste was mixed properly to get a good consistency of the paste. With the help of a squeegee, the paste placed inside the frame was then swiped onto the antenna design. The antenna design template as shown in the figure 21 was emulsed with the screen frame during the actual printing process.

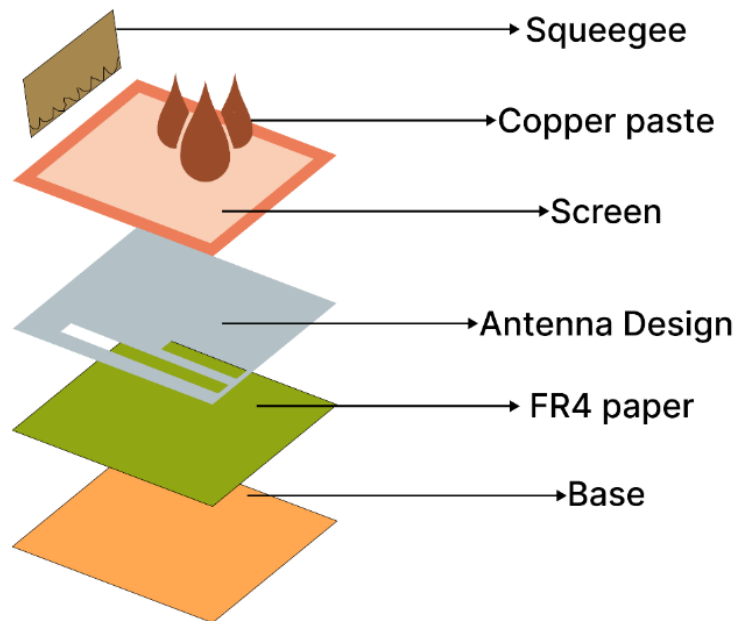


Figure 21. Process for the printing of antenna design

3.3.3 Post processing method for screen printing

Once the deposition of paste was completed in the substrate, the first thing we did with the samples was to make the deposition dry. For this, we put the samples on top of the thermal plate. The temperature was set at approx. 90°C for 7-10 seconds. This was followed by sintering process to achieve the conductivity. For this, thermal laminating company TLC 5500T 4” laminator was used. This specific laminator was set at 475°F for testing. The samples were placed inside the baking sheet, which acts as a carrier, and sent through the laminator machine. After the first pass through the laminator, the conductivity test was performed, and results were analyzed using VNA.

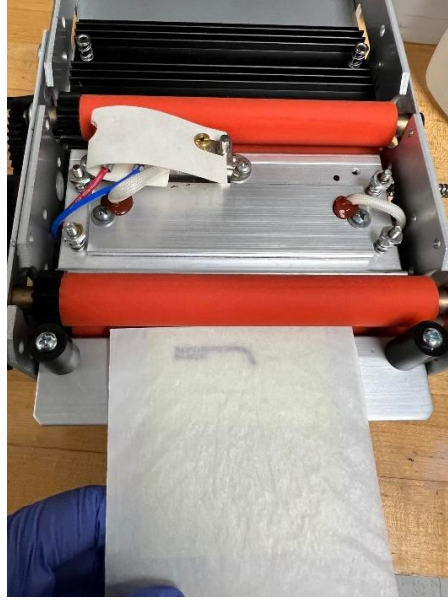


Figure 22. Post-processing method for screen printed antenna using laminator

3.4 PCB Fabrication – Method Used

All four antenna designs were also PCB fabricated for the purpose of comparison with two other fabrication method, AJP and screen printing. In the Ansys HFSS Electronics software, the design was extracted along its XY and YZ planes. Two coordinate planes were chosen, one at the bottom of the substrate and second at its top. The first coordinate was selected (for the bottom), and the substrate's ground plane was chosen. Then, the file was exported and saved in DXF format through the Modeler tab. Afterward, the second coordinate was selected (for the top), and the patch design was chosen and exported in DXF format. The two DXF files were re-imported into Ansys software, with the bottom file imported first and the layers were selected and saved. The top file was imported and saved on upper of the bottom one. Finally, the combined file is exported as a single DXF file.

3.4.1 PCB Design Layout Process

Since most PCB manufacturers require Gerber file format, the design DXF file extracted from Ansys HFSS was converted to Gerber format using KiCAD software. KiCAD is used to generate the necessary layers intended for the fabrication process. By opening the GerbView layout on KiCAD, the DXF file was imported from Ansys HFSS, and the required layers were selected and assigned per the manufacturer's specifications. After assigning the layers, the panelization process was performed based on the required quantity, and V-scoring is carried out using Mouse bites (2 mm) for easy separation after fabrication. The 3D Viewer was then used to preview the outcome before finally exporting the file in Gerber format and sending it to the chosen fabrication company. The company chosen for the fabrication of PCB board was Sunstone Circuits.

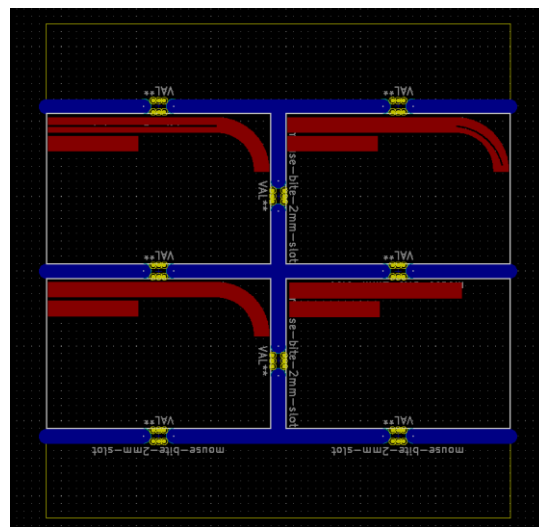


Figure 23. Design layout in GerbView

The final deposition pictures from both the printing process are shown in the next chapter along with the measurement of antenna parameters.

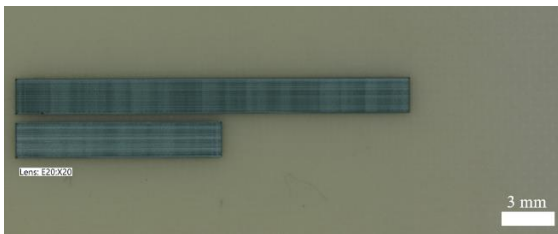
Chapter 4

Results and Discussion

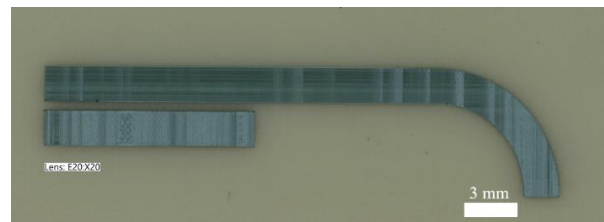
This chapter presents all the results from aerosol jet printing and screen printing and compares these with factory manufactured PCB boards. The reflection coefficient, an important antenna performance characteristic measured using Keysight VNA is explained broadly. The radiation pattern is another parameter measured from the simulation. The proposed antenna is also compared with a reference antenna on the basis of reflection coefficients and its application uses.

4.1 Antenna fabrication using AJP and Screen Printing

Microscopy images of the antenna design after the fabrication using aerosol jet printing and screen printing are shown in figure 24 and figure 25, respectively.



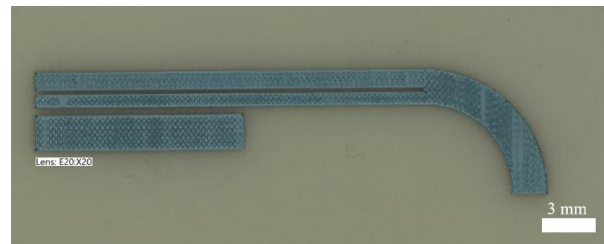
Design 1



Design 2

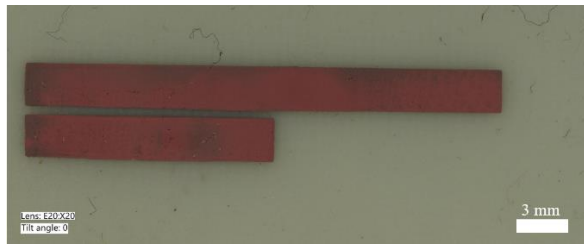


Design 3



Design 4

Figure 24. Four antenna design fabricated using aerosol jet printing



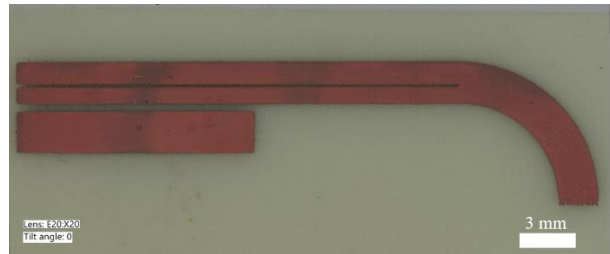
Design 1



Design 2



Design 3



Design 4

Figure 25. Four antenna design fabricated using screen printing

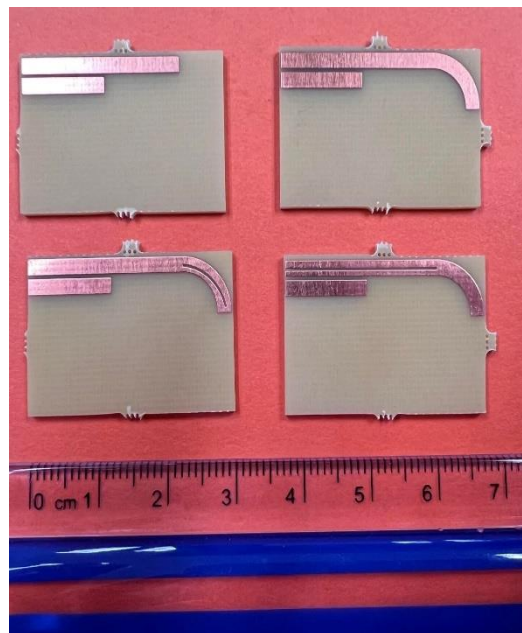


Figure 26. Factory manufactured antenna on a PCB Board

After the successful deposition, the fabricated antenna printed using both aerosol jet printing and screen printing were followed by post-processing method as explained in Chapter 3 to make it

conductive. The depth of the conductive part was measured on keyence microscope. For the AJP, the height of the conductive silver ink was about 10 μm and for screen printing, the height of copper paste turned out about 11 μm .

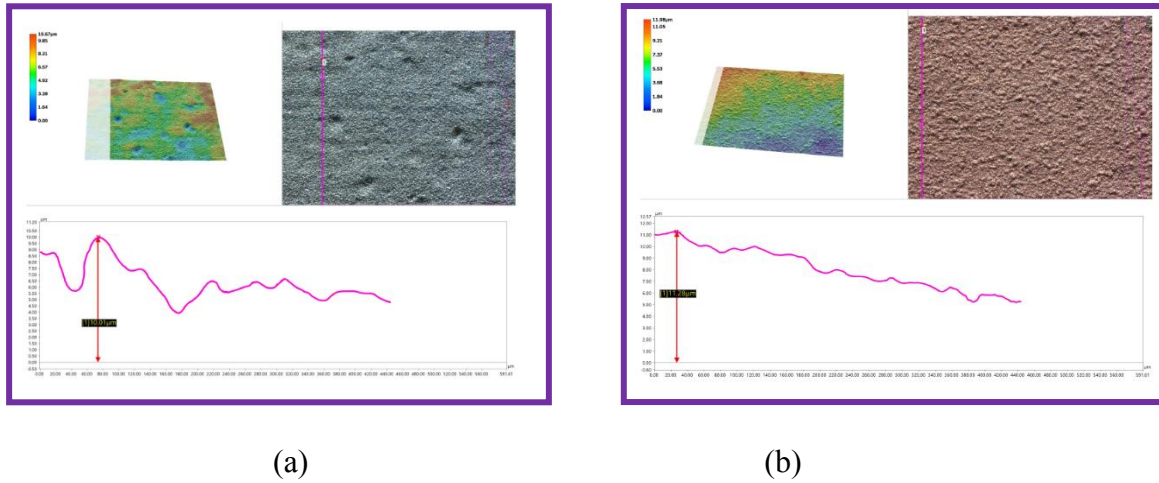


Figure 27. Measurement of the depth of conductive part using (a) AJP and (b) screen printing

After the deposition of ink were conductive, it was then tested using Keysight E5080B ENA VNA to study the antenna measurement like S-parameters (S11), resonant frequency, and bandwidth. SMA connector with a 50 Ω impedance is soldered to the feeding point of ACS-fed antenna. The factory manufactured PCB was also measured for the comparison.

4.2 Antenna Measurement

4.2.1 Reflection Coefficient

The reflection coefficient shows how much power is being reflected from the antenna and is measured by S11(dB). The antenna operates best when the S11 is less than -10 dB, transmitting 90% of the power, and the bandwidth is computed as a difference of higher frequency to lower frequency of S11 less than -10 dB [45]. The S11 characteristics in (dB) are measured over a wide

range of frequencies starting from 1 GHz to 20 GHz. All the graph results were plotted using the origin software and shown below from figure 28 to figure 35.

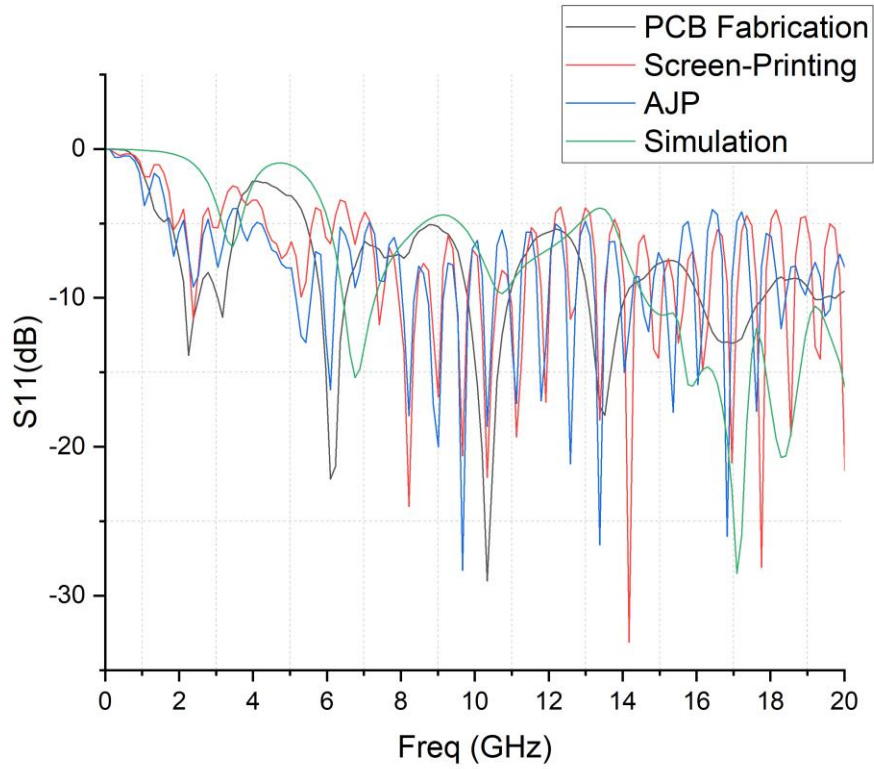
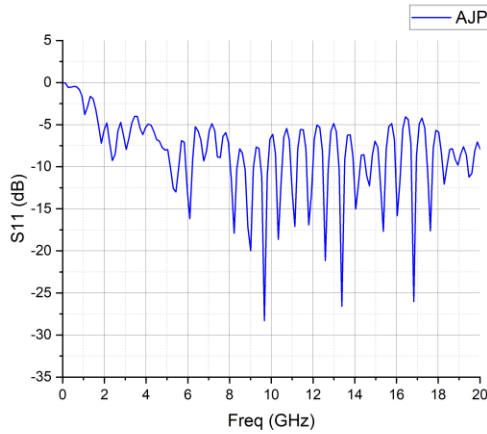
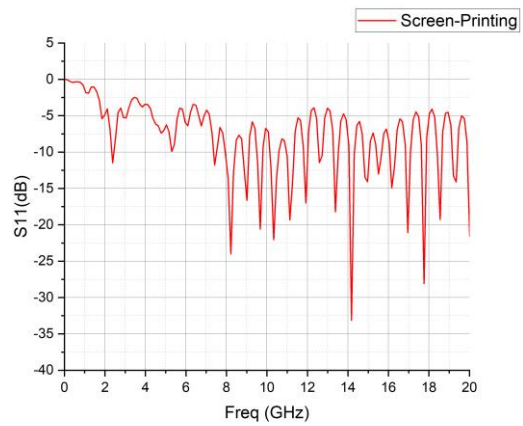


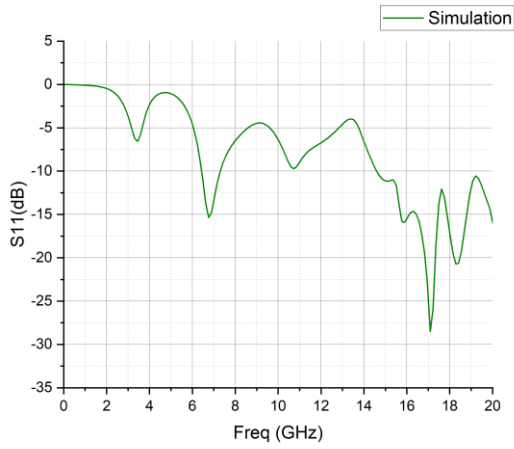
Figure 28. The PCB fabricated, simulated, screen printed and AJP reflection coefficient of antenna design 1



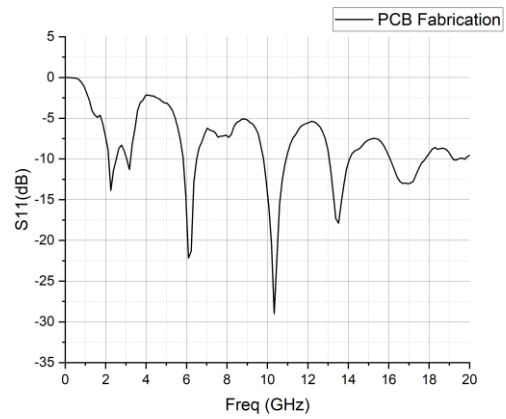
(a)



(b)



(c)



(d)

Figure 29. Reflection coefficient of (a) AJP, (b) Screen Printing, (c) Simulation, and (d) PCB fabrication of antenna design 1

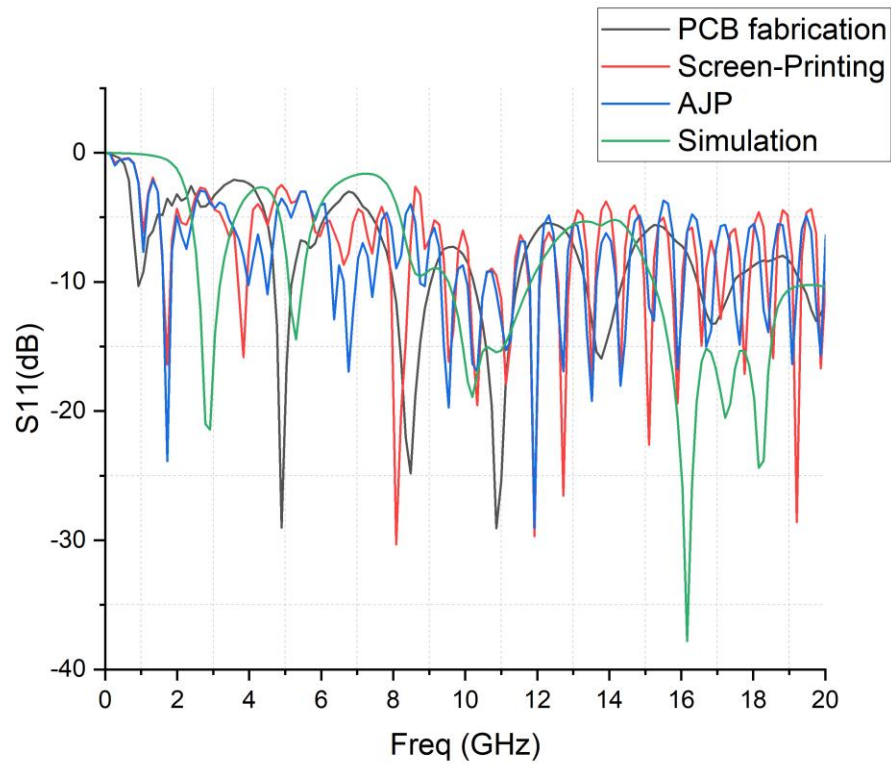
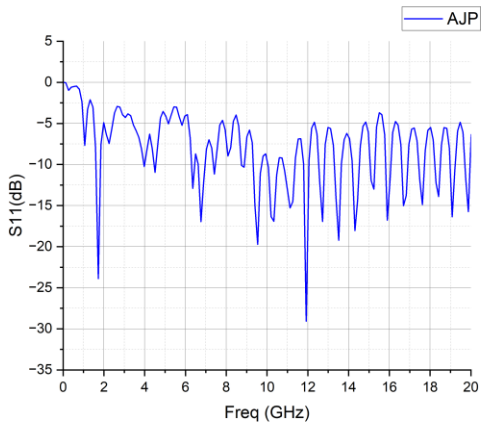
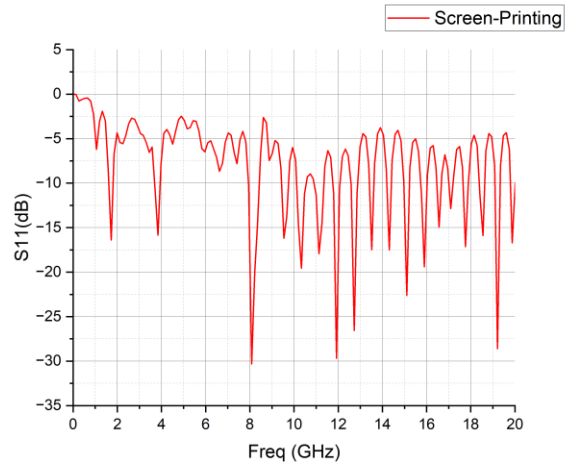


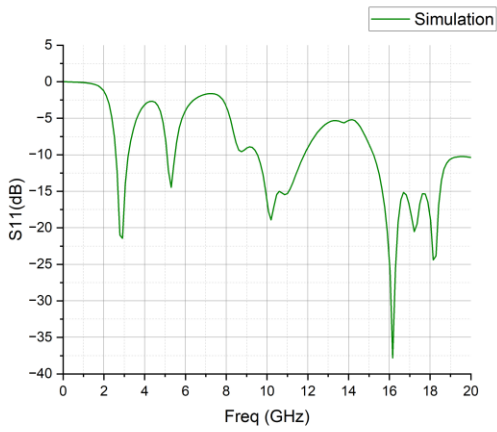
Figure 30. The PCB fabricated, simulated, screen printed and AJP reflection coefficient of antenna design 2



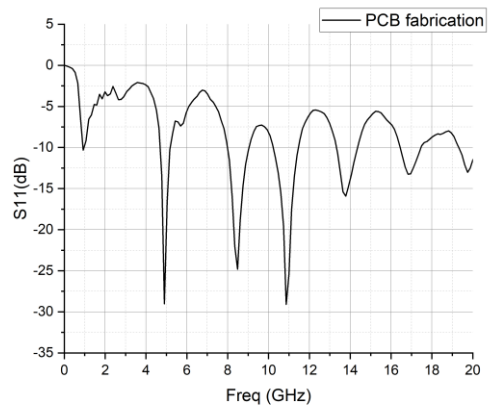
(a)



(b)



(c)



(d)

Figure 31. Reflection coefficient of (a) AJP, (b) Screen printing, (c) Simulation, and (d) PCB fabrication of antenna design 2

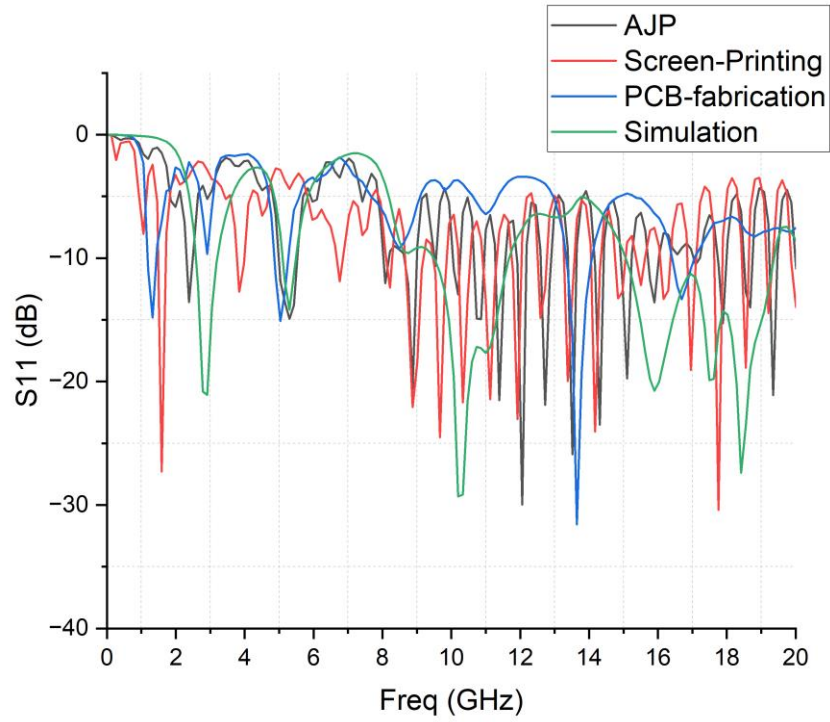
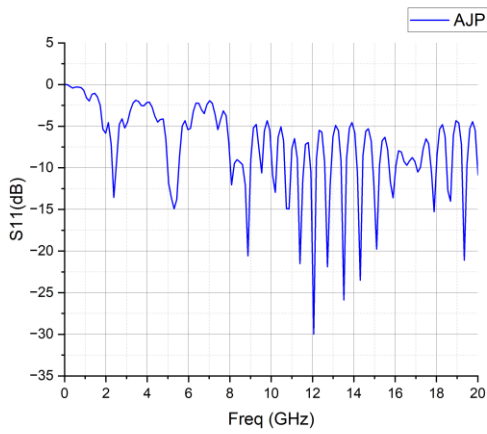
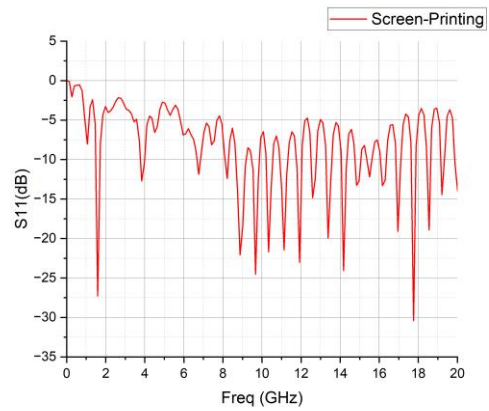


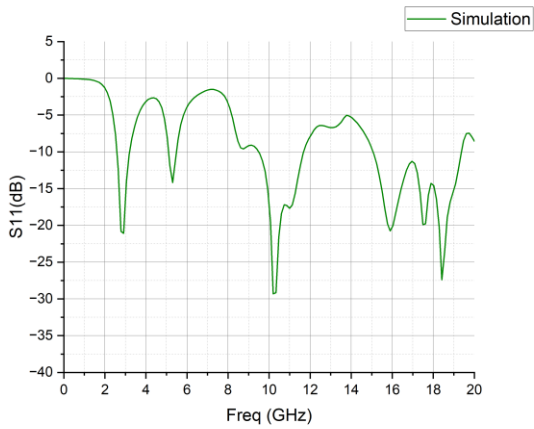
Figure 32. The PCB fabricated, simulated, screen printed and AJP reflection coefficient of antenna design 3



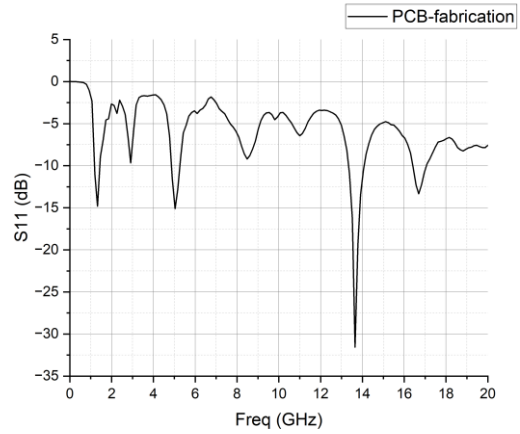
(a)



(b)



(c)



(d)

Figure 33. Reflection coefficient of (a) AJP, (b) Screen Printing, (c) Simulation, and (d) PCB fabrication of antenna design 3

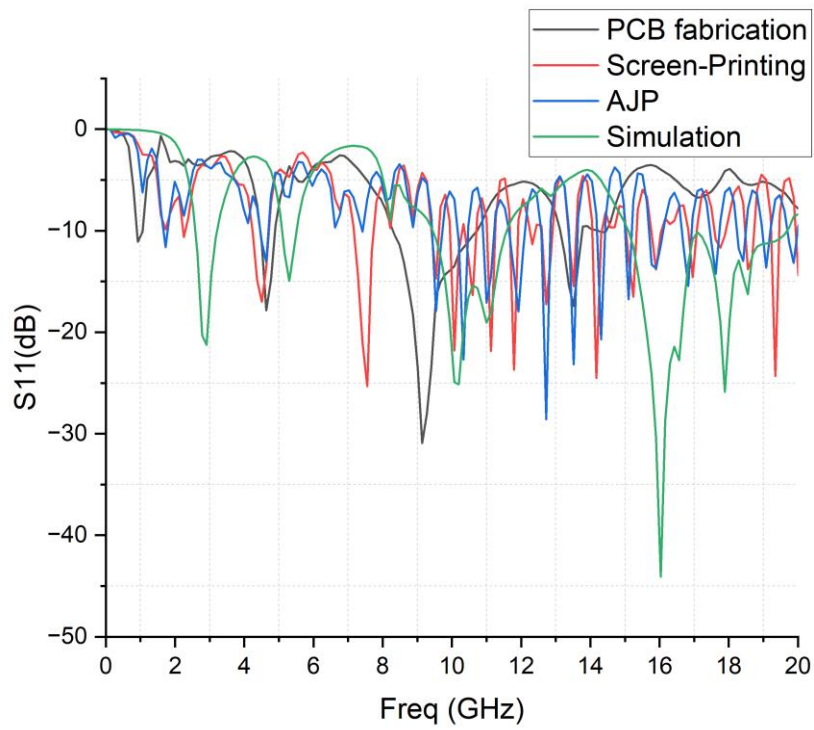
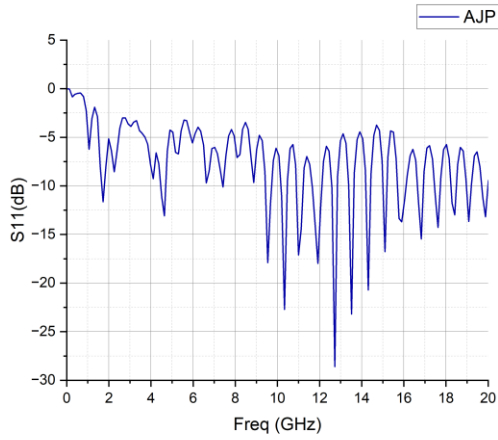
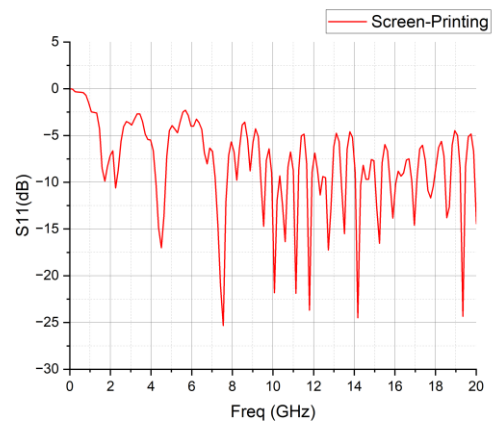


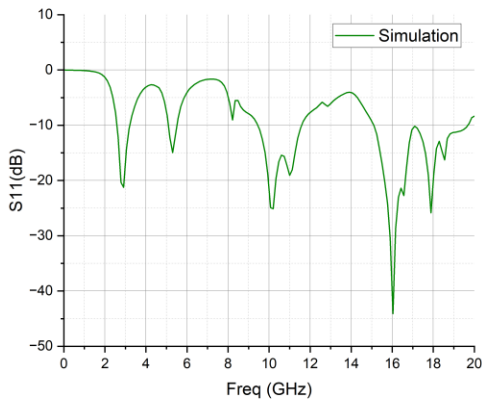
Figure 34. The PCB fabricated, simulated, screen printed and AJP reflection coefficient of antenna design 4



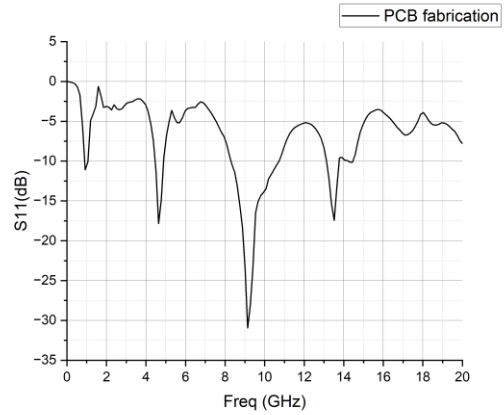
(a)



(b)



(c)



(d)

Figure 35. Reflection coefficient of (a) AJP, (b) Screen Printing, (c) Simulation, and (d) PCB fabrication of antenna design 4

Here, some of the S11 measurement result shows better return loss than the simulation which indicates that the fabricated antenna is best aligns with 50 ohm input impedance. The center frequency for the manufactured antenna and its corresponding bandwidth and S11 parameters are shown in the Table 4.

Table 4. Center frequency and its corresponding bandwidth and S11 parameters

| Design | AJP Center Freq (GHz) | BW(GHz) | S11(dB) | Screen-Printing Center Freq (GHz) | BW(GHz) | S11(dB) |
|----------|-----------------------|---------|---------|-----------------------------------|---------|---------|
| Design 1 | 6.09 | 0.3 | -16.17 | 8.21 | 0.48 | -24 |
| | 9.67 | 0.34 | -28.29 | 10.33 | 0.45 | -22.04 |
| | 13.38 | 0.26 | -26.59 | 14.17 | 0.26 | -33.13 |
| | 16.05 | 0.27 | -26.02 | 17.75 | 0.27 | -28.094 |
| Design 2 | 1.72 | 0.21 | -23.88 | 1.72 | 0.19 | -16.39 |
| | 6.75 | 0.37 | -16.95 | 8.08 | 0.5 | -30.31 |
| | 9.54 | 0.46 | -19.72 | 11.92 | 0.33 | -29.68 |
| | 11.92 | 0.26 | -29.07 | 15.1 | 0.24 | -22.62 |
| | | | | 19.21 | 0.24 | -28.59 |
| Design 3 | 8.87 | 0.39 | -20.58 | 1.59 | 0.25 | -27 |
| | 12.05 | 0.27 | -29.97 | 8.878 | 0.54 | -22 |
| | 13.51 | 0.26 | -25.89 | 9.68 | 0.41 | -21.69 |
| | 14.31 | 0.26 | -23.51 | 14.178 | 0.31 | -24.07 |
| | 19.34 | 0.25 | -21.11 | 17.75 | 0.24 | -30.39 |
| Design 4 | 4.63 | 0.24 | -13.08 | 2.25 | 0.06 | -10.63 |
| | 9.54 | 0.3 | -17.9 | 4.5 | 0.48 | -17 |
| | 12.72 | 0.28 | -28.66 | 7.55 | 0.59 | -25.32 |
| | 16.82 | 0.29 | -15.47 | 10.07 | 0.35 | -21.81 |
| | | | | 12.72 | 0.32 | -17.25 |
| | | | 14.17 | 0.28 | -24.56 | |

Here, the fractional bandwidth of an antenna is also calculated as it directly impacts the antenna's performance, versatility, and compatibility with various communication systems. It can be calculated using:

$$\text{Fractional bandwidth} = \frac{\text{Upper frequency} - \text{Lower frequency}}{\text{Center frequency}}$$

Fractional bandwidth provides insights into the range of frequencies over which the antenna can operate effectively, ensuring optimal signal fidelity, flexibility in accommodating signal variations, and mitigation of interference. A suitable fractional bandwidth can be tailored for specific communication systems, such as radar, satellite communications, or wireless networks,

enhancing system robustness and compatibility. Furthermore, a wider fractional bandwidth can increase channel capacity, allowing for the transmission of more data within the same timeframe, which is crucial for high-speed data transmission applications. In summary, the fractional bandwidth is a critical parameter for engineers and researchers in selecting or designing antennas that meet the requirements of specific applications and achieve optimal system performance. Here, for the Design 1 using AJP, the antenna has successfully achieved center frequencies of 6.09GHz, 9.67GHz, 13.38GHz and 16.05GHz with operational bandwidths ranging from 5.9 to 6.2 GHz, 9.49 to 9.83GHz, 13.24 to 13.5GHz and 15.94 to 16.21GHz, respectively. These bandwidths represent 4.92%, 3.51%, 1.94% and 1.68% fractional bandwidths respectively, indicating wideband performance capable of supporting various applications within any of the specified frequency ranges.

4.2.2 Radiation Pattern and 3D Polar Plot

Radiation pattern refers to the directional distribution of radiation from an antenna in three-dimensional space. It is a graphical representation of how the antenna radiates energy into free space. From the simulation, the radiation characteristics along H-plane and the 3D polar plot are measured and shown in figure 36- figure 39.

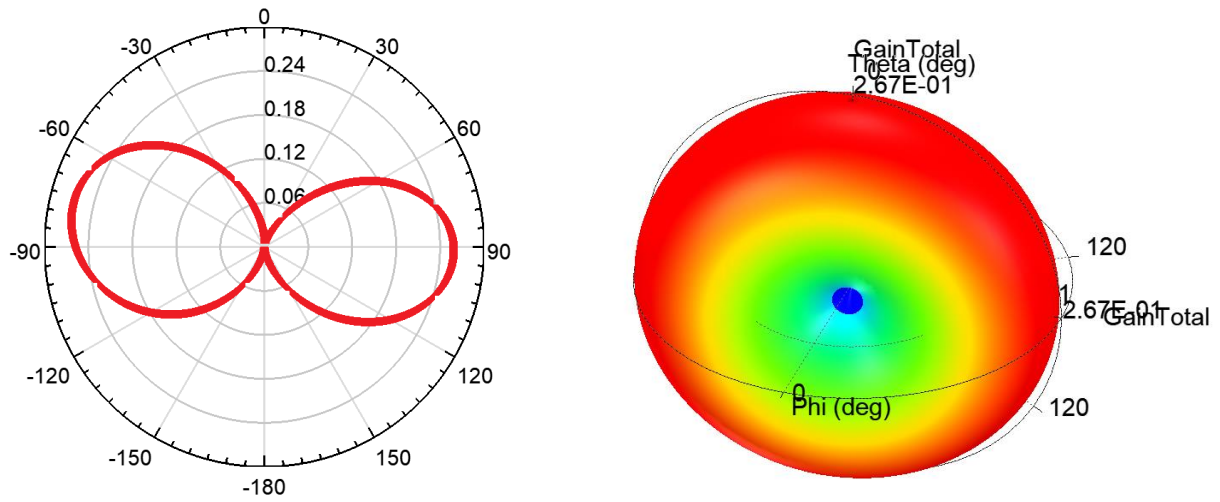


Figure36. Radiation pattern and 3D Polar Plot for Design 1

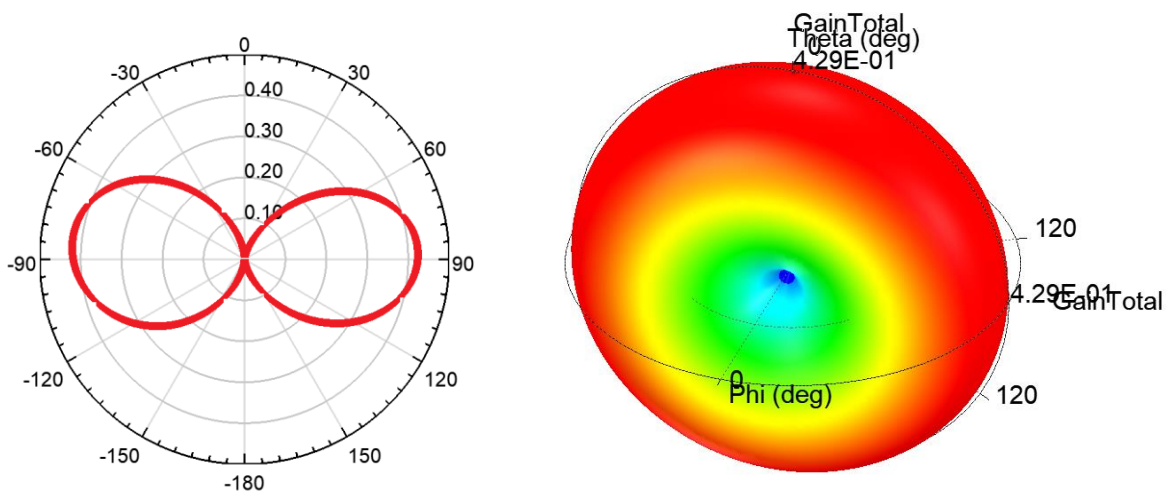


Figure 37. Radiation pattern and 3D Polar Plot for Design 2

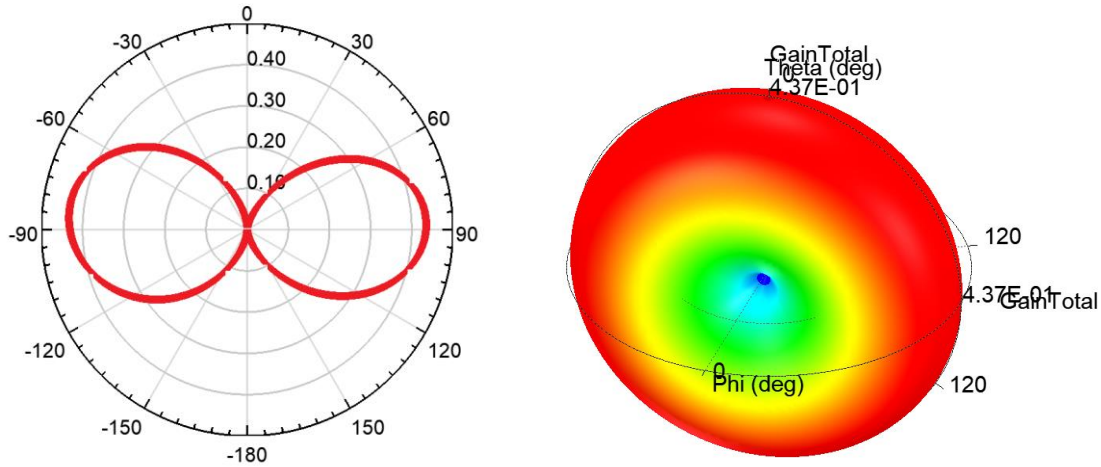


Figure 38. Radiation pattern and 3D Polar Plot for Design 3

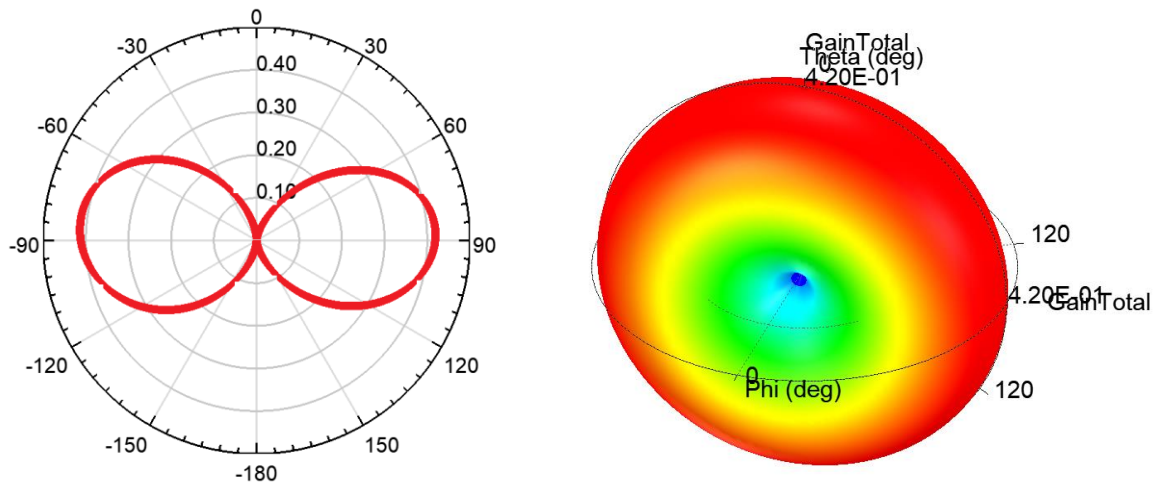


Figure 39. Radiation pattern and 3D Polar Plot for Design 4

The antenna exhibits an omni-directional radiation pattern and stable gain performance throughout the entire bandwidth, demonstrating its efficacy for reliable communication. Moreover, the compact size and fabrication simplicity of our antenna design contribute to its practicality and cost-effectiveness. Our findings reveal the potential of this antenna design for integration into a diverse array of biomedical applications, wireless communication systems, wearable sensors. Further

optimization and analysis of the antenna's electrical and mechanical properties can potentially unlock even greater performance and versatility in future iterations.

4.2.3 Reference Comparison Table

Table 5 shows the comparison with the reference antenna.

Table 5. Comparison of referenced antenna

| Reference | Dielectric Substrate | Frequency(GHz) | Return loss (dB) | Antenna Type | Application |
|-----------|--|--------------------------------|----------------------|--|--|
| [46] | FR4 substrate | 5.5,8.5 | -10.25, -15.25 | Circular Patch Antenna | Wireless Communication System |
| [47] | Roger's Kappa-438 substrate | 2.45,5.8, 10 | -18.88,-17.87,-19.26 | Microstrip monopole antenna | UWB application |
| [48] | Acrylonitrile Butadiene Styrene (ABS) resin with 3-D printing technology | 11.7-12.7 | -22,-12 | horn antenna | Radiometer Applications |
| [49] | ABS fingernail | 15.2 | -35 | microstrip patch antennas | 5G Applications |
| [50] | FR4 epoxy substrate | 2.025 | -22 | AMC-Based Dual band Microstrip Antenna | Wireless Communication |
| [51] | FR4 | 3.848 | -23.521 | Hash-Shape Slotted Microstrip Antenna | Future High-Speed 5G Wireless Communication Technology |
| [52] | Flexible conductive cloth MKKTN260 | 5.85 (with tissue measurement) | -23.5 | CPW-fed slot antenna | Medical wearable applications |
| [53] | flexible Liquid crystal polymer substrate | 2.5 | -24.5 | circular ring-shaped monopole antenna | Body-centric wearable applications |
| [54] | flexible polyethylene foam | 3.7 | -27 | Quad-Port UWB MIMO | Wearable Applications |

| | | | | | |
|------|-------------------------|------|--------|--|-----------------------------|
| | | | | Footwear Antenna | |
| [55] | FR4 substrate | 1.6 | -25.5 | flexible mild microwave hyperthermia antenna | Chemo-therapy of the Breast |
| [56] | FR4 epoxy | 10.3 | -27 | regular monopole shape rectangular patch antenna | Medical Application |
| [57] | Rogers substrate RO4350 | 10.3 | -24.57 | microstrip patch antenna | Radio Location Applications |

The proposed antenna can be compared with the reference table on the basis of frequency and return loss. In an application like wireless communication system [50], or a medical use like chemotherapy of the breast [55] where a lower frequency range 1-2 GHz is used, antenna design 2 fabricated using AJP can be employed. For breast cancer detection using radar-based [58] or a body centric wearable application [53], 2-4 GHz frequency is applied for which antenna design 3 using screen printing can be an alternative option. A number of applications is also explored in ultra-wide band frequency range to provide both an adequate depth of penetration and an image resolution which is reasonably high [59]. For that kind of application, both antenna design 1 and 2 using both fabrication methods can be a good option. For the application involving inter operative radiotherapy [56] or radio location application [57] where X-band or Ku Band of frequency range is suggested, antenna design 3 or 4 using screen printing fabrication method can be used. The K-band frequency can be utilized in an application where it is required to establish communication between implantable medical devices and external devices in a WBAN system using antenna design 3 fabricated by AJP.

Chapter 5

5.1 Summary and Conclusion

Two different additive manufacturing techniques, aerosol jet printing and screen printing have been studied and employed to fabricate antennas in this research. The four different antenna designs were designed and simulated in Ansys HFSS. For convenience of comparison, the substrate material, size, and thickness were all chosen as FR-4 substrate, 30 mm x 20 mm, and 0.1 mm, respectively. The fabrication procedure was carried out after all the antenna performance was adequately examined in the simulation.

For aerosol jet printing, several tests optimizing different parameters like sheath flow rate, atomizer flow rate, pressure, atomizer voltage, print speed were run to get a fine deposition. In addition to this, copper paste was used to fabricate an antenna using screen printing. After following the successful post-processing method, the samples were tested for antenna performance, namely reflection coefficient and resonant frequency using Keysight VNA.

All the antenna results show a good coverage of frequency band from L-band to K-band. The aim of the proposed antenna which was to achieve reflection coefficient below -10 dB while maintaining the bandwidth ≥ 100 MHz was fulfilled. The calculated fractional bandwidth indicates the wideband performance capable of supporting various applications in the specified frequency ranges. All these antennas can find applications in health monitoring systems, such as glucose monitoring and early detection of breast cancer cells at lower frequencies. At higher frequencies, it can be applied for wireless network applications.

5.2 Future Work

The completion of this research opens the door for many future possibilities. Firstly, it is recommended to scale down the design keeping every other parameter the same. These changes in the design can possibly bring the effectiveness of antenna in an applications like high-resolution radars, imaging systems, sensing, and high-speed communications by operating at THz frequencies. Secondly, we recommend investigating an alternative material and the post processing method by keeping the design and parameters same. These can be compared with this research work. Third, this work presents the design and fabrication of the antenna design. Future work could involve the integration of the antennas with sensors to create fully functional bio-medical and wearable devices.

Based on the present research's findings and limitations, these are only a few prospective topics for further exploration. Future study in these areas might help to eliminate some of the current limitations and broaden the scope of this work's possible uses.

References

- [1] T. Wohlers and T. Gornet, "History of Additive Manufacturing," 2016.
- [2] "The 7 Types of Additive Manufacturing - Carbon."
<https://www.carbon3d.com/resources/blog/the-7-types-of-additive-manufacturing> (accessed Apr. 02, 2023).
- [3] K. Sukanuma, "Introduction," pp. 1–22, 2014, doi: 10.1007/978-1-4614-9625-0_1.
- [4] S. Kirtania *et al.*, "Flexible Antennas: A Review," *Micromachines (Basel)*, vol. 11, p. 847, Mar. 2020, doi: 10.3390/mi11090847.
- [5] Y. Zhan, Y. Mei, and L. Zheng, "Materials capability and device performance in flexible electronics for the Internet of Things," *J. Mater. Chem. C*, vol. 2, no. 7, pp. 1220–1232, 2014, doi: 10.1039/C3TC31765J.
- [6] N. K. Nikolova, "Microwave Imaging for Breast Cancer," *IEEE Microw Mag*, vol. 12, no. 7, pp. 78–94, Dec. 2011, doi: 10.1109/MMM.2011.942702.
- [7] S. Symeonidis, W. G. Whittow, M. Zecca, and C. Panagamuwa, "Bone fracture monitoring using implanted antennas in the radius, tibia and phalange heterogeneous bone phantoms," *Biomed Phys Eng Express*, vol. 4, no. 4, p. 45006, May 2018, doi: 10.1088/2057-1976/aab974.
- [8] M. Asili *et al.*, "Flexible Microwave Antenna Applicator for Chemo-Thermotherapy of the Breast," *IEEE Antennas Wirel Propag Lett*, vol. 14, pp. 1778–1781, Feb. 2015, doi: 10.1109/LAWP.2015.2423655.
- [9] A. T. Mobashsher and A. Abbosh, "Microwave imaging system to provide portable-low-powered medical facility for the detection of intracranial hemorrhage," in *2014 1st Australian Microwave Symposium (AMS)*, Jun. 2014, pp. 23–24. doi: 10.1109/AUSMS.2014.7017347.
- [10] A. M. Abbosh, S. A. Rezaeieh, and K. Bialkowski, "Microwave techniques as diagnostic tool for congestive heart failure," in *2014 IEEE MTT-S International Microwave Workshop Series on RF and Wireless Technologies for Biomedical and Healthcare Applications (IMWS-Bio2014)*, Dec. 2014, pp. 1–3. doi: 10.1109/IMWS-BIO.2014.7032406.
- [11] S. Wiwatwithaya, P. Phasukkit, S. Tungjitkusolmun, and W. Wongtrairat, "Real-time monitoring glucose by used microwave antenna apply to biosensor," in *The 4th 2011 Biomedical Engineering International Conference*, Jan. 2012, pp. 135–137. doi: 10.1109/BMEiCon.2012.6172036.
- [12] Md. R. Robel, "Microwave antennas for biomedical application," RMIT University, 2019.
- [13] I. Gibson, D. Rosen, B. Stucker, and M. Khorasani, "Additive Manufacturing Technologies".
- [14] J.-P. Kruth, M. C. Leu, and T. Nakagawa, "Progress in Additive Manufacturing and Rapid Prototyping," *CIRP Annals*, vol. 47, no. 2, pp. 525–540, 1998, doi: [https://doi.org/10.1016/S0007-8506\(07\)63240-5](https://doi.org/10.1016/S0007-8506(07)63240-5).
- [15] G. N. Levy, R. Schindel, and J. P. Kruth, "RAPID MANUFACTURING AND RAPID TOOLING WITH LAYER MANUFACTURING (LM) TECHNOLOGIES, STATE OF THE ART AND FUTURE PERSPECTIVES," *CIRP Annals*, vol. 52, no. 2, pp. 589–609, 2003, doi: [https://doi.org/10.1016/S0007-8506\(07\)60206-6](https://doi.org/10.1016/S0007-8506(07)60206-6).
- [16] O. Abdulhameed, A. Al-Ahmari, W. Ameen, and S. H. Mian, "Additive manufacturing Challenges, trends, and applications," *Advances in Mechanical Engineering*, vol. 11, pp. 1–27, Mar. 2019, doi: 10.1177/1687814018822880.
- [17] H. Bikas, P. Stavropoulos, and G. Chryssolouris, "Additive manufacturing methods and modeling approaches: A critical review," *The International Journal of Advanced Manufacturing Technology*, vol. 83, Mar. 2015, doi: 10.1007/s00170-015-7576-2.

- [18] K. Suganuma, "Introduction to Printed Electronics," vol. 74, 2014, doi: 10.1007/978-1-4614-9625-0.
- [19] X. Zeng, C. Yang, J. F. Chiang, and J. Li, "Innovating e-waste management: From macroscopic to microscopic scales.," *Sci Total Environ*, vol. 575, pp. 1–5, 2017.
- [20] M. J. Tan, C. Owh, P. L. Chee, A. K. K. Kyaw, D. Kai, and X. J. Loh, "Biodegradable electronics: cornerstone for sustainable electronics and transient applications," *J. Mater. Chem. C*, vol. 4, no. 24, pp. 5531–5558, 2016, doi: 10.1039/C6TC00678G.
- [21] J. Wiklund *et al.*, "A Review on Printed Electronics: Fabrication Methods, Inks, Substrates, Applications and Environmental Impacts," *Journal of Manufacturing and Materials Processing*, vol. 5, no. 3, 2021, doi: 10.3390/jmmp5030089.
- [22] A. Kamyshny and S. Magdassi, "Conductive Nanomaterials for Printed Electronics," *Small*, vol. 10, no. 17, pp. 3515–3535, Sep. 2014, doi: 10.1002/SMLL.201303000.
- [23] Y. Khan, A. Thielens, S. S. Muin, J. Ting, C. L. Baumbauer, and A. C. Arias, "A New Frontier of Printed Electronics: Flexible Hybrid Electronics," *Advanced Materials*, vol. 32, 2019.
- [24] E. Kunnari, J. Valkama, M. J. Keskinen, and P. Mansikkamäki, "Environmental evaluation of new technology: printed electronics case study," *J Clean Prod*, vol. 17, pp. 791–799, 2009.
- [25] A. Nathan *et al.*, "Flexible Electronics: The Next Ubiquitous Platform," *Proceedings of the IEEE*, vol. 100, no. Special Centennial Issue, pp. 1486–1517, May 2012, doi: 10.1109/JPROC.2012.2190168.
- [26] E. B. Secor, "Principles of aerosol jet printing," *Flexible and Printed Electronics*, vol. 3, no. 3, p. 35002, Jul. 2018, doi: 10.1088/2058-8585/aace28.
- [27] "IDS NM." <https://www.idsnm.com/> (accessed Jan. 18, 2023).
- [28] A. Mahajan, C. D. Frisbie, and L. F. Francis, "Optimization of Aerosol Jet Printing for High-Resolution, High-Aspect Ratio Silver Lines," *ACS Appl Mater Interfaces*, vol. 5, no. 11, pp. 4856–4864, Jun. 2013, doi: 10.1021/am400606y.
- [29] "Products | UT Dots." <https://utdots.com/products> (accessed Jan. 28, 2023).
- [30] V. Mirshafiee, O. J. Osborne, B. Sun, and T. Xia, "Chapter 60 - Safety Concerns of Industrial Engineered Nanomaterials," in *Handbook of Nanomaterials for Industrial Applications*, C. Mustansar Hussain, Ed., in Micro and Nano Technologies. Elsevier, 2018, pp. 1063–1072. doi: <https://doi.org/10.1016/B978-0-12-813351-4.00062-6>.
- [31] R. R. Suresh *et al.*, "Fabrication of screen-printed electrodes: opportunities and challenges," *J Mater Sci*, vol. 56, no. 15, pp. 8951–9006, 2021, doi: 10.1007/s10853-020-05499-1.
- [32] R. Soukup, A. Hamáček, and J. Řeboun, "Advanced screen printing for the fabrication of organic humidity sensors," in *2012 4th Electronic System-Integration Technology Conference*, Sep. 2012, pp. 1–5. doi: 10.1109/ESTC.2012.6542183.
- [33] Z. Taleat, A. Khoshroo, and M. Mazloum-Ardakani, "Screen-printed electrodes for biosensing: a review (2008–2013)," *Microchimica Acta*, vol. 181, no. 9, pp. 865–891, 2014, doi: 10.1007/s00604-014-1181-1.
- [34] W.-C. Chang, L.-W. Weng, C.-K. Chuang, J.-X. Liang, T.-N. Yang, and W.-Y. Ma, "The Preparation of Antioxidant Copper Paste and Its Application to Silicon Solar Cells," *J Nanosci Nanotechnol*, vol. 16, pp. 9125–9131, Jan. 2016, doi: 10.1166/jnn.2016.12898.
- [35] "Nano Copper Paste for PET Substrates Application Notes", Accessed: Jan. 27, 2023. [Online]. Available: www.copprint.com
- [36] "Products – Copprint." <https://www.copprint.com/products/#LF-350> (accessed Jan. 21, 2023).

- [37] “PCB Manufacturing Process – A Step by Step Guide | PCBCart.” <https://www.pcbcart.com/article/content/PCB-manufacturing-process.html> (accessed Jan. 27, 2023).
- [38] “Ansys HFSS | 3D High Frequency Simulation Software.” <https://www.ansys.com/products/electronics/ansys-hfss#tab1-2> (accessed Apr. 08, 2023).
- [39] “Engineering Analysis With ANSYS Software”.
- [40] “Guide to FR-4 Printed Circuit Board (PCB) Material - NextPCB.” <https://www.nextpcb.com/blog/guide-to-fr-4-printed-circuit-board-material-nextpcb> (accessed Jan. 28, 2023).
- [41] “Digital Microscopes | KEYENCE America.” <https://www.keyence.com/products/microscope/digital-microscope/> (accessed Jan. 18, 2023).
- [42] “Network Analyzers | Keysight.” <https://www.keysight.com/us/en/products/network-analyzers.html> (accessed Jan. 18, 2023).
- [43] “E5080B ENA Vector Network Analyzer | Keysight.” <https://www.keysight.com/us/en/product/E5080B/e5080b-ena-vector-network-analyzer.html> (accessed Jan. 27, 2023).
- [44] “Microwave Frequency Bands.” <https://www.everythingrf.com/tech-resources/frequency-bands> (accessed Mar. 31, 2023).
- [45] Constantine A. Balanis, “Antenna Theory: Analysis and Design, 4th Edition | Wiley,” p. 1104, 2016, Accessed: Apr. 01, 2023. [Online]. Available: <https://www.wiley.com/en-us/Antenna+Theory%3A+Analysis+and+Design%2C+4th+Edition-p-9781118642061>
- [46] S. Kannadhasan and R. Nagarajan, “Performance Analysis of Circular Shape Microstrip Antenna for Wireless Communication System,” *IOP Conf Ser Mater Sci Eng*, vol. 1085, no. 1, p. 12013, Feb. 2021, doi: 10.1088/1757-899X/1085/1/012013.
- [47] B. Taha and H. Marhoon, “Simulation and manufacturing of modified circular monopole microstrip antenna for UWB applications,” *International Journal of Advances in Applied Sciences*, vol. 10, pp. 70–78, Mar. 2021, doi: 10.11591/ijaas.v10.i1.pp70-78.
- [48] L. Wu, H. Chu, D. Cao, S. Peng, and Y. Guo, “3-D Printed Antenna Subsystem With Dual-Polarization and its Test in System Level for Radiometer Applications,” *IEEE Access*, vol. 8, pp. 127856–127865, Mar. 2020, doi: 10.1109/ACCESS.2020.3008727.
- [49] P. Njogu, B. Sanz-Izquierdo, A. Elibiary, S. Y. Jun, Z. Chen, and D. Bird, “3D Printed Fingernail Antennas for 5G Applications,” *IEEE Access*, vol. 8, pp. 228711–228719, Mar. 2020, doi: 10.1109/ACCESS.2020.3043045.
- [50] M. F. Maulana, E. Ahmad Zaki Hamidi, A. Munir, and N. Ismail, “AMC-Based Dualband Microstrip Antenna for Wireless Communication,” in *2021 7th International Conference on Wireless and Telematics (ICWT)*, Aug. 2021, pp. 1–4. doi: 10.1109/ICWT52862.2021.9678498.
- [51] Md. S. Rana and Md. M. Rahman, “Design and Performance Evaluation of a Hash-Shape Slotted Microstrip Antenna for Future High-Speed 5G Wireless Communication Technology,” in *2022 6th International Conference on Trends in Electronics and Informatics (ICOEI)*, Apr. 2022, pp. 668–671. doi: 10.1109/ICOEI53556.2022.9776929.
- [52] Y. J. Li, Z. Y. Lu, and L. S. Yang, “CPW-Fed Slot Antenna for Medical Wearable Applications,” *IEEE Access*, vol. 7, pp. 42107–42112, Mar. 2019, doi: 10.1109/ACCESS.2019.2908199.
- [53] B. P. Nadh, B. T. P. Madhav, M. S. Kumar, T. A. Kumar, M. V. Rao, and S. S. M. Reddy, “MEMS-based reconfigurable and flexible antenna for body-centric wearable applications,” *J Electromagn Waves Appl*, vol. 36, no. 10, pp. 1389–1403, 2022, doi: 10.1080/09205071.2022.2028682.

- [54] S. Jayant, G. Srivastava, and S. Kumar, “Quad-Port UWB MIMO Footwear Antenna for Wearable Applications,” *IEEE Trans Antennas Propag*, vol. 70, no. 9, pp. 7905–7913, Sep. 2022, doi: 10.1109/TAP.2022.3177481.
- [55] M. Asili *et al.*, “Flexible Microwave Antenna Applicator for Chemo-Thermotherapy of the Breast,” *IEEE Antennas Wirel Propag Lett*, vol. 14, pp. 1778–1781, Feb. 2015, doi: 10.1109/LAWP.2015.2423655.
- [56] S. Ramya and P. Vijayalakshimi, “A Low Cost X-Band UWB Antenna for Medical Application: Optimal Design and Analysis,” in *2018 International Conference on Communication and Signal Processing (ICCSP)*, Apr. 2018, pp. 14–17. doi: 10.1109/ICCSP.2018.8524219.
- [57] A. S. Bhadouria, S. Kumari, and M. Kumar, “X-Band and Ku-Band Patch Antenna for Radio Location Applications,” *Proceedings of the International Conference on Recent Cognizance in Wireless Communication & Image Processing*, pp. 897–904, 2016, doi: 10.1007/978-81-322-2638-3_101.
- [58] X. Yun, E. C. Fear, and R. H. Johnston, “Compact antenna for Radar-based breast cancer detection,” *IEEE Trans Antennas Propag*, vol. 53, no. 8, pp. 2374–2380, Aug. 2005, doi: 10.1109/TAP.2005.852308.
- [59] X. Li, S. C. Hagness, M. K. Choi, and D. W. van der Weide, “Numerical and experimental investigation of an ultrawideband ridged pyramidal horn antenna with curved launching plane for pulse radiation,” *IEEE Antennas Wirel Propag Lett*, vol. 2, pp. 259–262, Feb. 2003, doi: 10.1109/LAWP.2003.820708.


```

99     </enable_fans>
100     <nozzle_max_volumes_per_sec type="float">
101         <item>300</item>
102     </nozzle_max_volumes_per_sec>
103     <nozzle_temps_max type="float">
104         <item>0</item>
105     </nozzle_temps_max>
106     <z_speeds_max type="float">
107         <item>30</item>
108     </z_speeds_max>
109     <e_speeds_max type="float">
110         <item>200</item>
111     </e_speeds_max>
112     <xy_speeds_max type="float">
113         <item>200</item>
114     </xy_speeds_max>
115     <extruder_offsets type="float">
116         <item x="0" y="0" z="0"/>
117     </extruder_offsets>
118 </fff_settings>
119 </additive>
120
121 <axis actuator="linear" coordinate="Y" homePosition="0mm" id="Y" link="table" maximumFeed="0mm/min" name=""
122 offset="0mm 0mm 0mm" rapidFeed="0mm/min" resolution="0mm"/>
123
124 <axis actuator="linear" coordinate="X" homePosition="0mm" id="X" link="table" maximumFeed="0mm/min" name=""
125 offset="0mm 0mm 0mm" rapidFeed="0mm/min" resolution="0mm"/>
126
127 <axis actuator="rotational" axis="1 0 0" control="driven" coordinate="X" cyclic="no" homePosition="0deg" id="U" link="table" maximumFeed="2160deg/min" name=""
128 offset="0mm 0mm 0mm" preference="dont care" range="0deg 360deg" rapidFeed="0deg/min" reset="previous" resolution="0deg" tcp="yes"/>
129
130 <axis actuator="rotational" axis="0 0 1" control="driven" coordinate="Z" cyclic="no" homePosition="0deg" id="V" link="table" maximumFeed="2160deg/min" name=""
131 offset="0mm 0mm 0mm" preference="dont care" range="0deg 360deg" rapidFeed="0deg/min" reset="previous" resolution="0deg" tcp="yes"/>
132
133 <axis actuator="linear" coordinate="Z" homePosition="0mm" id="Z" link="head" maximumFeed="0mm/min" name="" offset="0mm 0mm 0mm" rapidFeed="0mm/min" resolution="0mm"/>
134
135 <spindle axis="0 0 1" maximumSpeed="0rpm" minimumSpeed="0rpm">
136     <description></description>
137 </spindle>
138
139 </machine>
140

```

The G-code generation for the antenna design 1 is shown below:

```
1 ;Iteration1
2 ;Printer name: IDS Nanojet
3 ;Print time: 40m:21s
4 ;Extruder 1 material used: 14mm
5 ;Extruder 1 material name:
6 ;Extruder 1 nozzle diameter: 0.05mm
7 ;Extruder 1 offset x: 0mm
8 ;Extruder 1 offset y: 0mm
9 ;Extruder 1 offset z: 0mm
10 ;Extruder 1 max temp: 0
11 ;Layer count: 10
12 ;Width: 150mm
13 ;Depth: 150mm
14 ;Height: 300mm
15 ;Count of bodies: 2
16 ;Fusion version: 2.0.14793
17 ;Set Delays for Gcode
18 REAL #ONDELAY
19 REAL #OFFDELAY
20 REAL #PRIMEDELAY
21 #ONDELAY=0.15
22 #OFFDELAY=2
23 #PRIMEDELAY=15
24 ;-----
25 ;Selected Profile: Nanojet 25 Micron New
26 ;-----
27 ;Selected Printer: IDS, Nanojet
28 ;-----
29 T0
30 ;-----
31 ;Part 1
32 ;Layer : 1 of 10
33 ;rapid-dry
34 G1 F3000
35 G21
36 G90
37 Z0
38 G1 Z0.05 F6000
39 X0 Y0
40 G1 X0 Y-3 Z0 F2500
41 M201 M211 G04 X#PRIMEDELAY
42 M200 M210 G04 X#OFFDELAY
43 G0 X-22.985 Y-19.985 Z0.05
44 M201 M211 G04 X#ONDELAY
45 G1 F1500
46 ;bead-perimeter_outer
47 G1 X-0.015 F300
48 G1 Y-18.015
49 G1 X-22.985
50 G1 Y-19.985
51 G1 F1500
52 ;rapid-dry
53 G1 F3000
54 M200 M210 G04 X#OFFDELAY
55 G0 X-11.985 Y-17.485
56 M201 M211 G04 X#ONDELAY
57 G1 F1500
58 ;bead-perimeter_outer
59 G1 X-0.015 F300
60 G1 Y-15.515
61 G1 X-11.985
62 G1 Y-17.485
63 ;rapid-leaky
64 G1 F3000
65 M200 M210 G04 X#OFFDELAY
66 G0 X-0.039 Y-17.435
67 M201 M211 G04 X#ONDELAY
68 ;bead-sparse_infill
69 G1 X-11.961 F600
70 G1 Y-17.405
71 G1 X-0.039
72 G1 Y-17.375
73 G1 X-11.961
74 G1 Y-17.345
75 G1 X-0.039
76 G1 Y-17.315
77 G1 X-11.961
78 G1 Y-17.285
79 G1 X-0.039
80 G1 Y-17.255
81 G1 X-11.961
82 G1 Y-17.225
83 G1 X-0.039
84 G1 Y-17.195
85 G1 X-11.961
86 G1 Y-17.165
87 G1 X-0.039
88 G1 Y-17.135
89 G1 X-11.961
90 G1 Y-17.105
91 G1 X-0.039
92 G1 Y-17.075
93 G1 X-11.961
94 G1 Y-17.045
95 G1 X-0.039
96 G1 Y-17.015
97 G1 X-11.961
98 G1 Y-16.985
99 G1 X-0.039
100 G1 Y-16.955
101 G1 X-11.961
102 G1 Y-16.925
103 G1 X-0.039
104 G1 Y-16.895
105 G1 X-11.961
106 G1 Y-16.865
107 G1 X-0.039
108 G1 Y-16.835
109 G1 X-11.961
110 G1 Y-16.805
111 G1 X-0.039
112 G1 Y-16.775
113 G1 X-11.961
114 G1 Y-16.745
115 G1 X-0.039
116 G1 Y-16.715
117 G1 X-11.961
118 G1 Y-16.685
119 G1 X-0.039
120 G1 Y-16.655
121 G1 X-11.961
```